

The following publication Wan, Z., Sun, Y., Tsang, D. C., Hou, D., Cao, X., Zhang, S., ... & Ok, Y. S. (2020). Sustainable remediation with an electroactive biochar system: mechanisms and perspectives. Green Chemistry, 22(9), 2688-2711 is available at <https://doi.org/10.1039/D0GC00717J>.

1 **Green and sustainable remediation with electroactive biochar system: Mechanisms**
2 **and perspectives**

3

4 Zhonghao Wan¹, Yuqing Sun¹, Daniel C.W. Tsang^{1,*}, Deyi Hou², Xinde Cao³, Shicheng Zhang⁴, Bin Gao⁵,
5 Yong Sik Ok⁶

6 ¹Department of Civil and Environmental Engineering, The Hong Kong Polytechnic University, Hong Kong, China

7 ²School of Environment, Tsinghua University, Beijing 100084, China.

8 ³School of Environmental Science and Engineering, Shanghai Jiao Tong University, 800 Dongchuan Road, Shanghai
9 200240, China.

10 ⁴Shanghai Key Laboratory of Atmospheric Particle Pollution and Prevention (LAP3), Department of Environmental
11 Science and Engineering, Fudan University, Shanghai 200438, China

12 ⁵Department of Agricultural and Biological Engineering, University of Florida, Gainesville, FL 32611, United States.

13 ⁶Korea Biochar Research Center & Division of Environmental Science and Ecological Engineering, Korea University,
14 Seoul 02841, Republic of Korea.

15

16 * Corresponding author email: dan.tsang@polyu.edu.hk

17

18 **Abstract**

19 Biochar functionalized with electroactive components is triggering increasing attention owing to its
20 versatile redox roles and tuneable structural configurations. In this review, we summarise and highlight
21 the electrochemical properties of biochars with various theoretical, methodological, and experimental
22 manners, and offer new perspectives on electrochemical carbocatalysis of biochars to guide future
23 environmental applications. Electrochemical carbocatalysis is for the first time correlated with the
24 synergistic effects among reactive-active moieties (RAMs), metal contents, defective sites, heteroatoms
25 doping, and conductive graphitic surface within manoeuvrable biochar framework for biochar-involved
26 environmental interactions. It is worth noting that milder redox reactions including the formation of
27 surface-confined reactive complexes, singlet oxygenation, and direct electron transfer can be properly
28 introduced with specific protocols, thus minimizing undesirable carbon oxidation and enhancing reaction
29 sustainability. Overall, this review presents future research directions on mechanistic aspects of
30 electroactive components on biochar to facilitate its applications in sustainable carbocatalysis and green
31 chemistry.

32 1. Introduction

33 Confronted with the tremendous demand for environmental remediation due to the prevailing
34 anthropogenic activities (*e.g.*, atmospheric pollution, soil deterioration, and water contamination),¹
35 cutting-edge technologies based on green heterocatalysts are triggering intensive interests from human
36 kind to envisage a sustainable future.² The over-discharged hazardous substances in industrial wastewater
37 and diverse biowastes have transcended the natural degradation capacity and remain as severe
38 environmental threats.³⁻⁵ In recent years, state-of-the-art remediation technologies utilizing heterogeneous
39 materials for the adsorption and catalytic degradation of various pollutants have been extensively
40 investigated and applied in different fields such as soil amendment and decontamination,⁶⁻¹⁰ carbon
41 sequestration,¹¹⁻¹³ water/wastewater treatment,¹⁴⁻²¹ and so forth.

42 Versatile carbon-based materials showing merits such as abundance on earth, superior mechanical
43 strength, tuneable physicochemical properties (surface area, pore structure, and electrical conductivity,
44 *etc.*), and ease of scaling-up, have stimulated great impetus for development of heterogeneous catalysts.¹
45 ^{2,22-28} Compared with homogeneous/heterogeneous catalysis using transition metals and their oxides, *e.g.*,
46 iron,²⁹ cobalt,³⁰ or manganese.^{21, 31} heterogeneous carbon-based materials have shown eminent
47 preponderance *via* either directly interacting with pollutants by inherent reactive-active moieties (RAMs)
48 or producing highly reactive oxygen species (ROS) to degrade organic contaminants into harmless
49 substances (*i.e.*, salt ions, carbon dioxide, and H₂O).^{20, 25, 32-37} The latest development of efficient
50 carbocatalysis based on the inherent chemical or structural active sites of various carbonaceous materials
51 (including graphene, carbon nanotubes, nanodiamonds, mesoporous carbon, and graphitic carbon nitride,
52 *etc.*) can provide alternative candidates to overcome the deficiencies in metal-based advanced oxidation
53 processes (*i.e.*, AOPs). This scope echoes with the growing emphasis on cleaner process and sustainable
54 demand in environmental field, which is especially highlighted in this review.

55

56 Biochar, a pyrogenic black carbon manufactured under oxygen-limited conditions, has drawn
57 enormous attention and inspired a wide array of investigations to exploit its versatile intrinsic properties
58 in green and environmental remediation.^{38, 39} Emerging as a green, environmentally benign, easily
59 accessible, and effective granular carbonaceous material developed from refractory biomass wastes,
60 biochar can be applied in agricultural, environmental, and biorefinery fields. It is a prospective alternative
61 to replace the costly nanocarbons and template-based carbocatalysts, which generally need cost- and
62 chemical-intensive synthetic procedures under harsh conditions with a low yield.⁴⁰⁻⁴³ With respect to the
63 specific features (low energy input, carbon footprint, life-cycle environmental impact, *etc.*) for green and
64 sustainable remediation, biochar or engineered biochar stands out for its facile manufacture, value-added
65 nature, and excellent sustainability in field-scale applications.

66 Nowadays, environmental utilization of biochar has been driven by its promising potential of resistance
67 to pH change, nutrient retention capacity, mitigation of climate change (*e.g.*, CO₂, CH₄, and N₂O),
68 contaminant adsorption capability, value-added conversion catalysis, and compatibility as catalyst
69 support.^{16, 17, 40, 44-49} Attributed to the accessible active sites and manoeuvrable porous structure, biochar
70 has been investigated as an efficient and cost-effective adsorbent for immobilization of various
71 metals/metalloids and organic pollutants.^{11, 50} Nevertheless, the adsorbed macromolecules cannot be
72 completely degraded. End-of-service-life disposal/regeneration of spent adsorbents and secondary
73 contamination risk inevitably impedes its field application.⁵¹ Irrespective of the convenient accessibility
74 and modification for biochar, its surface area, pore distribution and volume, as well as hydrophobicity of
75 biochar surface are still limited when compared with activated carbon or nanocarbon materials.⁵² The
76 regime using biochar as adsorbent has met an insurmountable bottleneck for environmental
77 decontamination.

78 Intriguingly, the role of the redox reactivity of biochars in green and sustainable remediation are being
79 continuously noticed.^{7, 19, 53} It is recognized that some typical RAMs, *i.e.*, amino –NH_x and phenolic –OH,

80 with abundant unconfined electrons can contribute to the degradation of pollutants,⁵⁴ while ketonic group
81 (C=O) with high electron density facilitates plausible catalysis due to its nucleophilic nature.^{2,55} Multiple
82 electron-mediated pathways upon environmentally persistent free radicals (EPFRs) have also been
83 elucidated.⁵² EPFRs with unpaired electrons are validated to possess reactivity to either directly degrade
84 inorganic/organic pollutants or stimulate the generation of ROS.⁵⁶ Theoretical modelling by density
85 functional theory (DFT) further illustrates that defective sites (edge sites, vacancy defects, and voids, *etc.*)
86 and distorted carbon species that maintain intact sp^2 -hybridization and confine π -electrons and spins in
87 localized area can demonstrate high catalytic potential.⁵⁷ In addition, metal-biochar composites can
88 incorporate various metal components (*i.e.*, metal or metal oxide) to promote electron transition,^{18, 58-64}
89 while the application of active metal-functionalized biochars unavoidably induces metal leaching into the
90 environment, which is potentially detrimental to clean water source and requires prudent pollution
91 control.^{20, 65} The incorporation of exogenous non-carbon atoms are also triggering immense and
92 momentous movement to activate graphitic biochar with well-ordered carbon matrices.^{36,55} Accordingly,
93 the highly graphitized structure of biochar may inspire future sustainable technologies with the
94 involvement of heteroatoms doping technology.²

95 To date, many review papers have provided in-depth investigation of biochar applications,^{40, 45, 46, 66-82}
96 most of which focused on either the preparation or modification processes of biochars, and correlated with
97 crop production, soil amendment, carbon sequestration, or value-added products conversion.
98 Nevertheless, the existing reviews only emphasized conventional physicochemical properties for better
99 adsorption capacity, *i.e.*, surface area, pore filling adsorption/partition, complexation *via* functional groups,
100 cation exchange capacity, hydrophobic interaction, and π - π interaction, *etc.* The foregoing electron-
101 mediated scenarios on biochar are partially understood and poorly interconnected, especially for the
102 potential pivotal synergistic effects among each critical electroactive component within biochar matrices.
103 Therefore, this review aims to foster future inspirations of cutting-edge biochar research.

104 We critically review the latest progress in the electron-mediated regime applied in environmental
105 remediation, for the purpose of articulating the key sustainable issues including identification of reactive
106 species, selective enrichment of active sites, and manipulation of reaction pathways (e.g., radical or non-
107 radical) in the view of experimental, methodological, and theoretical aspects. The scope covers from the
108 ubiquitous and mature skills (i.e., optimization of RAMs and metal active sites) to the highlighted green
109 and emerging technologies (i.e., manipulation of defective level, heteroatoms, and conductive carbon
110 matrices). We hope to cultivate new insights and accelerate growth of wider applications of engineered
111 biochar with the emphasis on green and sustainable remediation.

112

113 2. Modulated electron transfer regime from RAMs on biochar

114 In recent studies, RAMs on biochar have been reported to exhibit good electrochemical reactivity for
115 water/wastewater treatment and soil decontamination, which consists of the active and abundant free-
116 flowing electrons along the biochar peripheries.⁸³ Due to the variable surface chemistry and
117 nonstoichiometric nature of biochars derived from diverse biomass with uncontrollable components,² it
118 has been long debated which component of RAMs should be superior and preferable to govern the redox
119 process. Some RAMs with strong affinity towards pollutants tend to exhibit weak stability and selectivity,
120 while the other longstanding RAMs somehow show milder and sustainable capacity under specific
121 circumstances. This requires insightful understanding of biochar-derived environmental application, e.g.,
122 AOPs, to probe the multiple catalytic pathways by RAMs and enable advanced optimization in biochar
123 preparation.

124 **Table 1** lists the common RAMs on biochar that could be determined by basic characterization methods
125 and were reported to be catalytic for pollutant degradation. RAMs on biochar could be generally
126 categorized into two types, namely electron-rich functional groups and inherent EPFRs. The generation
127 of functional groups mainly results from incomplete decomposition or cleavage of

128 hemicellulose/cellulose/lignin/protein or hydrolysis of organic compounds during ionic reactions.^{84, 85} In
129 comparison, the formation of EPFRs usually originates from a series of reactions including initial
130 [physisorption](#), elimination of water or hydrogen chloride, and subsequent electron transfer from
131 substituted aromatic units to adsorbed transition metals. The formation of EPFRs would occur in this
132 process accompanied by the reduction of metal centres.^{37, 52, 56} The incorporation of transition metals
133 (intrinsic mineral ash content or exogenous metal additives) could manifest catalytic performance by
134 tuning the density and diversity of both functional groups and EPFRs.⁸⁶ As a result, the synergistic effects
135 among metal centres and organic components account for the characteristics of RAMs on biochar.

136 **2.1. Formation of RAMs in biochar**

137 **2.1.1. General formation of RAMs**

138 Biochar can be produced by pyrolysis (*i.e.*, pyrochar) or hydrothermal process (*i.e.*, hydrochar) under
139 limited oxygen or anoxic conditions, wherein massive dangling RAMs could be generated along with the
140 structural defects on carbon matrices. Hydrothermal carbonization process is usually conducted at a
141 relatively low temperature around 160–300 °C and an autogenic high pressure between 200–600 Bar. The
142 ionic reaction between biomass and water-induced ions (*i.e.*, hydronium and hydroxide ions) dominated
143 under subcritical conditions. Specifically, the high-weight organic compounds with long chains are
144 catalytically hydrolysed to form oligomers and monomers, subsequently undergoing condensation,
145 carbonization, re-polymerization, and aromatization to form hydrochar. Substantial oxygen-containing
146 RAMs with high reactivity and unconfined electrons would be generated during these hydration and
147 fragmentation processes.⁸⁷ Comparatively, biochar fabricated from pyrolytic process tends to be
148 functionalized with modulated types and quantity of functionalities due to the [thermal](#) instability of
149 respective groups. Greater graphitization degree can be also achieved with higher pyrolytic temperature.
150 More inner RAMs could be exposed due to the volatilization of condensable hydrocarbons during

151 pyrolysis. Besides, the articles on gasification biochar for green and environmental remediation are still
152 insufficient,^{10,47,88} which would be excluded from this review.

153 **2.1.2. Impact from inherent substances on functionalization**

154 Biochars with distinct physicochemical properties could also originate from many different sources,
155 including lignin- and cellulose-rich wood/bark/husk/shell/straw/stem from forestry and agricultural
156 industries, ash-rich sludge/litter/manure from livestock farmyard and wastewater treatment plants,
157 protein- or hydrocarbon-rich microbe/tissue/rubber/polymer from biofuel, cosmetic, and food industries,
158 or other particular carbon-rich biomass. The selection of feedstock significantly influences both the
159 original types and quantity of RAMs on the resultant biochar. Generally, biomass with high lignin content
160 would lead to higher biochar yields and well-ordered carbon structure, which is favourable for the
161 preservation and formation of RAMs with lower dissolved organic matters. Biochars derived from
162 biomass with high ash content (*i.e.*, sludge and manure) are subject to functionalization with catalytic
163 metal components acting as pore forming agents or exterior electron donors. Metal content also helps to
164 catalyse the generation of EPFRs and modulate yield and types. The formation of EPFRs could be
165 ascribed to the transition metals which absorb on biomass surface and mediate electron transfer from
166 polymers to metal centres during pyrolysis. However, a pyrolytic temperature above 700 °C would
167 diminish almost all electron paramagnetic resonance (EPR) signal peaks assigned to EPFRs as a result of
168 the elimination of oxygen functionalities, suggesting the important role of oxygen moieties possessing
169 rich free-flowing electrons with paramagnetic properties.³⁶ Fang et al. found both the introduction of metal
170 contents (*i.e.*, Ni, Cu, Zn, and Fe) and phenolic compounds (*i.e.*, hydroquinone, catechol, and phenol)
171 favour EPFRs formation in biochar. The overdose of metal contents presented a negative effect on density
172 of EPFRs, and the consummation of EPFRs was attributed to the self-reduction reactions of metal ion
173 centres and EPFRs. Similarly, phenolic compounds would also induce oxidation or reduction side-effects
174 when transcending the optimal concentrations.⁸⁹

175 2.1.3. Crucial impact of thermal conditions

176 It is well known that the pyrolytic and hydrothermal conditions (*i.e.*, peak temperature, retention time,
177 and ramping rate) can act as the crucial factors during the formation of multiple functional groups (*i.e.*,
178 aromatic, aliphatic, and phenolic groups) on biochar.⁸⁵ Amongst, pyrolysis temperature plays a vital role
179 on the density of functional groups on biochar. Low-temperature biochar (200–350 °C) was observed
180 with high density of oxygen-containing groups, while types and amounts of functional groups could be
181 tailored with moderate temperature level (350–700 °C).³⁸ Specifically, (a)
182 lignin/cellulose/protein/polymer tend to dehydrate/cleave at lower temperature (200–350 °C) to form
183 dense RAMs on the surface of carbon structure; (b) lignin/cellulose/protein/polymer-derived
184 transformation products would abruptly decompose at mid-range temperature (350–700 °C) and the
185 presence of aromatic functionalities could be observed, leading to a lower RAMs diversity; (c)
186 carbonization and graphitization are increasing at higher temperature (700–900 °C), removing almost all
187 RAMs.⁹⁰ Similarly, peak temperature also significantly influences the properties of resultant hydrochar in
188 subcritical reactions. For cellulose decomposed within temperature range from 220–300 °C, products with
189 denser functionalities such as water-soluble sugars (oligomers and monomers) could be obtained by
190 dissolution and hydrolysis of cellulose, and carboxylic acids, ketones, and aldehydes obtained by
191 dehydration of sugars are primarily observed.⁹¹ [The condensation, repolymerization, and aromatization](#)
192 [will initiate at ~250 °C to cause](#) the formation of char, gases, and bio-oil (acetone-soluble phase), leading
193 to less RAMs on resultant hydrochar.⁹² Furthermore, Ruan et al. reviewed that the conversion of oxygen-
194 centred EPFRs into oxygenated carbon-centred radicals or carbon-centred type would occur at high
195 temperature.⁵² Precursor radicals of EPFRs usually form from homolytic cleavage of α - and β -alkyl aryl
196 ether, C–C, as well as C–O bonds, which vary with temperature to generate corresponding products. The
197 generated intermediate products are prone to couple and abstract hydrogen from other molecules, in which
198 the reaction conditions (*i.e.*, temperature, pressure, and residence time) are considered to govern the

199 sequential reactions, such as dehydration, decarboxylation, carbonization, aromatization, and intra-
200 molecule condensation.⁹³ The EPFRs density on corn straw-derived biochar pyrolyzed at 300 °C was 3.97
201 $\times 10^{18}$ spins g^{-1} while those of biochars derived from pine needle (P), wheat straw (W), maize straw (M),
202 and rice husk (R) were 13.7×10^{18} spins g^{-1} for P550 (indexed to pine needle derived biochar with
203 pyrolytic temperature 550 °C), 16.5×10^{18} spins g^{-1} for W400, 28.6×10^{18} spins g^{-1} for W500, 6.25×10^{18}
204 spins g^{-1} for M400, 30.2×10^{18} spins g^{-1} for M500, 2.77×10^{18} spins g^{-1} for R300, 17.1×10^{18} spins g^{-1}
205 for R500, and 0.16×10^{18} spins g^{-1} for R700, respectively.^{89, 94, 95} Besides, rice husk-derived biochar
206 induced by microwave at 1 kW for 30 min attained 8.94×10^{17} spins g^{-1} , indicating the disparities of
207 different heating approaches. Gao et al. also investigated the crucial factors of the hydrothermal
208 conversion from 180 to 270 °C for EPFRs generation on rice straw, and found EPFRs density exhibited
209 a unimodal trend with the richest active moieties centred at 240 °C. Then the intensity decreased abruptly
210 due to the condensation, aromatization, and repolymerization of carbon contents at higher temperature.⁹⁶
211 Overall, the yield and categories of EPFRs on biochar are mainly dominated by the temperature condition
212 corresponding to the decomposition of radical precursor.^{89, 97} The impacts of various operational
213 conditions are summarized and illustrated in **Fig. 1**.

214 In addition to peak temperature, heating rate and residence time are another two critical parameters.
215 Zhao et al. found residence time had medium effect on the density of functional groups, while no effect
216 could be found for diversity of functionalities on rapeseed-derived biochar.⁸⁵ The formation of EPFRs
217 during hydrothermal process was also time-dependent, and the density decreases with the increase of
218 residence time. This might be due to the greater decomposition/loss/leaching of phenolic compounds in
219 hydrochar, or the self-consumption with a prolonged reaction in the saturated biomass feedstock.⁸⁷
220 Moreover, optimal feedstock loading of solid biomass was also considered to be conducive to RAMs
221 generation in the hydrothermal process, which benefited to reach the complete pyrolysis/hydrolysis of
222 biomass particles.^{52, 80} Comparatively, ramping rate rarely influenced the RAMs formation in pyrolysis.

223 With respect to hydrothermal conversion process, pressure generally corresponds to the fluctuation of
224 reaction temperature, leading to the change of aqueous medium properties, which may inhibit or
225 accelerate reactions influencing RAMs formation.⁶⁶ It has also been reported that residence time and
226 solvent selection would result in the transformation of functional groups on hydrochar with varied
227 carbonization degree.⁹⁸ It is worth noting that cellulose conversion into primary products (oligomers and
228 monomers) does not require long residence time, while complete carbonization with longer hydrothermal
229 duration favours higher functionalization and yield of hydrochar. The specific formation processes for
230 functionalities and EPFRs in hydrothermal carbonization are depicted in **Fig. 2**.

231 **2.2. Electroactive catalysis with functional groups**

232 **2.2.1. The evolution of geobattery theory**

233 Phenolic –OH is firstly unveiled as electron donor to stimulate H₂O₂ to evolve ROS for the degradation
234 of various pollutants. Such phenomenon has been elucidated on model carbon-based materials in the
235 mitigation of greenhouse gas emission, iron mineral reduction, and organic pollutant decontamination.⁹⁹⁻
236 ¹⁰² Klupfel et al. verified the critical role of quinone/hydroquinone pairs and established a sophisticated
237 analytical method to quantify the redox capacity and electrochemical reversibility of black carbons, which
238 laid the foundation of electroactive biochar.¹⁰³ Yang et al. proposed that phenolic –OH on biochar made a
239 significant contribution to the direct reduction of *p*-nitrophenol, and the electron-donating ability of –OH
240 group in phenols promoted the preferential electrophilic attack on ortho- and para-positions of organic
241 compounds.¹⁰⁴ Recently, the discovery of ‘geobattery’ theory ([reversible functional interspecies](#)
242 [conversion](#)) on natural pyrogenic carbon, whereby phenolic –OH and quinoid C=O can undergo electron-
243 mediated transformation, further indicates the electron donating ability of phenolic –OH.^{105, 106} The
244 geobattery theory has been used to account for the enhanced microbial redox transformations of
245 contaminants (*e.g.*, acetate and nitrate).¹⁰⁷ Similar to iron redox cycles in natural magnetic minerals,

246 phenolic –OH in hydroquinone could couple with quinone content to reversibly accept and donate charges
247 between redox-active compounds.

248 **2.2.2. Reversible redox cycle of several key oxygen functionalities on biochar**

249 Considering the commonality of RAMs on different carbon-based structure, phenolic –OH on biochar
250 is expected to function very similarly to the natural organic matter in relevant biogeochemical and
251 environmental redox reactions.⁵⁴ Xin et al. investigated the capacity of a wood-derived biochar to mediate
252 redox processes in natural and engineered systems utilizing electron storage capacity (ESC) as index
253 parameter, and found biochar matrices could function as typical geobattery to store/release electrons.¹⁰⁸
254 Zhong et al. carefully verified the different roles of RAMs, *i.e.*, phenolic –OH, semiquinone-type EPFRs,
255 and quinoid C=O, in the oxidation of As(III). Borohydride and hydrogen peroxide were employed to
256 accomplish the facile interspecies conversion among different oxidized functional groups (OFGs, *e.g.*,
257 quinoid C=O) and reduced functional groups (RFGs, *e.g.*, phenolic –OH and semiquinone-type
258 EPFRs).⁵⁴ Besides, Wu et al. considered phenolic –OH on rice straw biochar might act as the electron-
259 transfer mediator to generate and release radicals as described in Eq. (1), and highly-active and electron-
260 lacking holes seemed to dominate the redox reactions.¹⁰⁹ The hole theory was supported by He et al. on
261 sawdust biochar, as holes generated on highly graphitized structure appeared to be responsible for the
262 formation of electron-donor/transfer complex.¹¹⁰ Considering the fact that holes are not likely to form
263 within biochar matrices due to the relative electroneutrality from zero band gap, the lack of inherent
264 highest occupied molecular orbitals (HOMO) and lowest occupied molecular orbitals (LOMO), and
265 uncertain efficiency of ethylenediaminetetraacetic acid (EDTA) as holes scavenger on carbon-based
266 system, the hole theory is considered to be the deviation and misapprehension from geobattery theory.



268 Nevertheless, the phenolic –OH/ketonic C=O redox cycle cannot be readily achieved and it
269 theoretically presents easily consumable properties susceptible to redox reactions. Accordingly, Kemmou

270 et al. deemed the hydroxyl groups on spent malt rootlets-derived biochar surface should play a vital role
271 *via* direct donation of electrons to stimulate the generation of persulfate radicals (*i.e.*, $\text{SO}_4^{\cdot-}$) for
272 sulfamethoxazole degradation with a remarkable consumption of $-\text{OH}$ groups.¹¹¹ Similar reaction
273 pathway was proposed in another wood-based biochar/peroxides system conducted by Zhu et al., where
274 phenolic $-\text{OH}$ was considered responsible for the formation of surface-bound reactive radicals.¹¹²

275 **2.2.3. Versatile role of ketonic C=O group on simplified carbonaceous materials**

276 More interestingly, multiple electron-mediated pathways upon ketonic C=O group on carbocatalysis
277 were progressed lately. Sun et al. first reported reduced graphene oxide (rGO), as a typical simplified
278 carbon model, could stimulate peroxymonosulfate (PMS, $\text{HO}-\text{OSO}_3^-$) to evolve radicals (*i.e.*, $\text{SO}_4^{\cdot-}$) for
279 the degradation of phenolics and dyes. Edge sites and ketonic groups at the carbon peripheries were found
280 to be chemically electroactive.¹¹³ With the help of density functional theory (DFT) modelling, Wang et al.
281 employed two typical carbon-based systems, *i.e.*, carbon spheres and rGOs, to clarify the specific
282 contributions of three different types of oxygen-containing functionalities ($-\text{C}=\text{O}$, $-\text{OH}$, and $-\text{COOH}$)
283 and found that the electroactivity mainly originated from the ketonic C=O groups on the aromatic
284 clusters.¹¹⁴ Theoretically, the PMS molecule ($\text{HO}-\text{OSO}_3^-$) was able to be cleaved into $\text{SO}_4^{\cdot-}$ over ketonic
285 C=O group.⁵⁷ Duan et al. also identified electroactive C=O group as the electron-rich sites, though Oh et
286 al. claimed ketonic C=O group should be electron-lacking saturated bond and is more inclined to accept
287 electrons.⁸³ Therefore, more experimental and theoretical validation is still required for the present
288 research elucidating the role of ketonic C=O group on carbon-based structures.

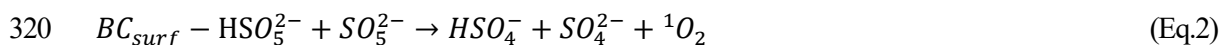
289 **2.2.4. Sustainable catalysis of ketonic C=O group on well-ordered biochar**

290 Our recent work revealed that biochar pyrolyzed under high temperature (900 °C) and carbon dioxide
291 medium possessed higher density of ketonic C=O groups.⁵⁵ In many cases, high pyrolytic temperature
292 above 700 °C would eliminate almost all oxygen-containing functional groups and lead to the
293 condensation/carbonization/graphitization of carbon clusters.³⁶ However, the introduced ketonic C=O

294 groups under this distinct phenomenon (*viz.* Boudouard reaction taking place at ≥ 710 °C: $C + CO_2 \rightarrow$
295 $2CO$) ruled out the interferences of other oxygen functionalities, and it was proven to be highly reactive
296 to activate peroxydisulfate (PDS, $^-O_3SO-OSO_3^-$) than the intrinsic honeycomb basal plane on biochar.
297 The introduction of ketonic C=O groups was also found on porous graphene using CO_2 as the activation
298 medium.¹¹⁵ Intriguingly, the reactive species generated in this process were mild and sustainable species
299 such as singlet oxygen (1O_2) with greater selectivity to electron-rich organics and less surface oxidation
300 on carbon matrices as compared to the conventional radical species (*i.e.*, $^{\bullet}OH$, $SO_4^{\bullet-}$, and $^{\bullet}O_2$).²⁵

301 Similar CO_2 activated-biochar produced from cellulose at 950 °C also confirmed the crucial role of
302 ketonic C=O groups to activate PMS to generate 1O_2 .¹¹⁶ Wang et al. considered that the ketonic C=O
303 groups terminated at carbon boundaries have unpaired electrons and tend to interact with PMS molecules
304 *via* inner-sphere interaction (C=O–H–O– OSO_3) to weaken the peroxide oxygen-oxygen bond.¹¹⁴ Same
305 scenario on CNTs could also be taken as reference, as Zhang et al. described a theoretical/experimental
306 method for the oxidative dehydrogenation of various organic compounds, which involved catalytic
307 cleavage of specific bonds driven by electron-transfer over active oxygenated functional groups
308 (enhanced and tailored by HNO_3 oxidation) attached to CNTs.¹¹⁷ Thus, ketonic C=O group was verified
309 to make the major contribution to directly attack electron-lacking saturated bonds due to their nucleophilic
310 nature with high electron cloud density. Herein, biochar-based geobattery theory should be more suitable
311 to explicate the critical role of ketonic C=O groups combined with recent exploration on phenolic –OH
312 group. As shown in **Figs. 3** and **4**, the ketonic groups with higher electron density would directly donate
313 electrons *via* inner-sphere interaction from its ketonic oxygen to the weakened O–O bond in peroxides
314 (*e.g.*, H_2O_2 , PMS, and PDS) to form metastable oxyanion-carbon complexes. The energy barrier of
315 peroxide dissolution is expected to decrease. The metastable oxyanion-carbon complexes would react
316 with another peroxide molecule to produce 1O_2 under mild conditions (**Eq. 2**). The positively charged
317 ketone groups would react with another peroxide molecule to produce distinct radicals (*e.g.*,

318 peroxymonosulfate radical and peroxydisulfate radical), and further regains charges to restore the ketonic
319 C=O groups from hydroquinone-type groups and fulfil the redox cycles of geobattery theory.²



321 **2.2.5. Redox cycle of nitrogenous functionalities**

322 In addition to the distinctive RAMs like phenolic –OH and ketonic C=O groups that can form a
323 geobattery pairs to readily mediate electrons, some other RAMs in carbocatalysis have also been noticed
324 to take effect in redox environmental applications. Ma et al. claimed polyethylenimine (PEI) modified
325 biochar could reduce hexavalent chromium Cr(VI) under acidic environment, where the introduced PEI
326 layer outside the biochar matrix with large amounts of amine-derived groups (–NH₂) played the crucial
327 role¹¹⁸. In the following research on m-phenylenediamine modified chitosan for Cr(VI) removal, Wan et
328 al. further substantiated the concurrent reduction-adsorption of Cr(VI) stemmed from the introduced
329 amino groups. Nitrogenous functional groups (*e.g.*, –NH–, =N–, –NH₂⁺–, and =NH⁺–) were found to
330 fulfil redox cycle within.¹¹⁹ Besides, aminated graphene functionalized with dense amino groups as
331 electron-donating functionalities was utilized to activate PDS, confirming the reductive role of amino
332 groups on carbonaceous materials.¹²⁰ It is worthy to note that oxynitride groups (–NO_x) with high
333 oxygenated contents in passivated carbonaceous materials were reported to be irreversibly ineffective for
334 electron-mediated reactions,¹²¹ which might indicate the nonstoichiometric nature of amino groups-
335 involved carbocatalysis.

336 **2.3. Electroactive catalysis based on EPFRs**

337 **2.3.1. General characteristics of EPFRs**

338 EPFRs have triggered **much** attention as another typical series of RAMs. EPFRs with unpaired
339 electrons, as the by-products formed after the incomplete thermal decomposition **under the catalysis of**
340 **transition metals** with half lives in ambient air from hours to months, have been reported to possess highly
341 active redox properties to catalyse peroxides (*e.g.*, H₂O₂, PMS, and PDS) to generate ROS *via* a single-

342 electron transfer process.^{52, 122, 123} Compared with the conventional free radicals released in bulk solution,
343 EPFRs are solid-phase free radicals confined on carbon structure and can induce the formation of oxidized
344 adducts sensitive to EPR detection.¹²⁴ Usually, EPFRs can be classified into three different classes with
345 Landé g-factor as indicator, namely carbon-centred type (g-factor < 2.003), carbon-centred type with an
346 adjacent oxygen atom (2.003 < g-factor < 2.004), and oxygen-centred type (2.004 < g-factor).¹²⁵ Oxygen-
347 centred radicals are generated from C–O bond cleavage and/or the introduction of oxygen atom within
348 the broken bonds, and they are relatively stable in air condition. Comparatively, carbon-centred type
349 EPFRs are more prone to free oxygen oxidation in air or dissolved state.¹²⁶ Specifically, cyclopentadienyls
350 (g-factor < 2.003), phenoxy radical (2.003 < g-factor < 2.004), and semiquinone radicals (2.0045 < g-
351 factor) are their typical representatives, respectively.⁵²

352 Fang et al. revealed that oxygen-centred radicals were the predominant species under relatively low
353 pyrolytic temperature (300–550 °C) and short residence time (1–2 h).⁸⁹ They could be decayed or
354 transformed into carbon-centred radicals with an adjacent oxygen atom or carbon-centred type as
355 temperature and residence time further increased. The g-factor of corn straw-derived biochar prepared at
356 300 °C was 2.004, resulting from semiquinone-type oxygen-centred radical,⁹⁴ while that of rice husk-
357 derived biochar prepared with similar pyrolysis process was 2.0038, verified to be characteristics of
358 oxygenated carbon-centred radical.⁵⁶ The types of EPFRs in biochar varied with different preparation
359 conditions and could be manipulated with controlled conditions to meet specific demands.

360 2.3.2. Nucleophilic attack with electron donation

361 Recently, EPFRs in biochars have been extensively noticed for their catalytic performance in various
362 environmental applications. Prompted from researches on ubiquitous activated carbon (AC) induced
363 hydrogen peroxide activation to generate highly active $\cdot\text{OH}$,¹²⁷ Fang et al. hypothesized and proved the
364 similar properties on biochar (prepared from wheat, pine needles, and maize straw with pyrolytic
365 temperature around 300–350 °C) as that of AC due to the existence of solid-phase resonance-stabilized

366 radicals, namely EPFRs, to stimulate the generation of $\cdot\text{OH}$ for 2-chlorobipheyl degradation.¹²⁸ The
367 mechanistic route was predominantly controlled by one-electron transfer from EPFRs towards H_2O_2
368 molecules, which was confirmed by a linear correlation among EPFRs density, $\cdot\text{OH}$ characteristic signal
369 intensity, as well as pollutant degradation rate constant. Subsequently, Fang et al. further confirmed the
370 critical role of EPFRs during the generation of $\cdot\text{OH}$ by biochar-induced dissolved oxygen activation, and
371 per molecule of $\cdot\text{OH}$ would lead to a consumption of around 12 spins of EPFRs.⁸⁹ The proposed ROS
372 generation pathways primarily came from the EPFRs-induced oxygen molecules activation to produce
373 $\cdot\text{O}_2^-$ and $\cdot\text{OH}$, while both these two radicals would consume free electrons on residual EPFRs to produce
374 more $\cdot\text{OH}$. Meanwhile, Yang et al. reported the reductive degradation of *p*-nitrophenol *via* EPFRs-induced
375 electron transfer, demonstrating the efficient, mild, and direct electron-delivery regime from EPFRs in
376 biochars.¹⁰⁴ This reductive capacity of carbon-centred EPFRs in biochar was also claimed by Zhong et al.,
377 as the simultaneous Cr(VI) adsorption-reduction could be achieved *via* direct electron donation without
378 additional peroxide addition.⁵⁶ Zhao et al. demonstrated similar EPFRs consumption on corn straw
379 biochar to reduce Cr(VI) in solution as accompanied by the formation of quinone groups, suggesting the
380 reversible electron donor-acceptor scenario of different RAMs on biochars.⁹⁴ New insights were fostered
381 by Zhong et al. recently, wherein phenolic $-\text{OH}$, semiquinone-type EPFRs, and ketonic $\text{C}=\text{O}$ groups were
382 regarded to form geobattery pairs as fully reduced, intermediate, and fully oxidized form of quinone
383 structure, respectively, which can reversibly donate and accept charges accompanied by the release and/or
384 consumption of protons.⁵⁴ These findings corroborated the interspecies connections among O-
385 functionalities and EPFRs, and provided new direction to manipulate and modulate the electroactive
386 components in biochar.

387 **2.3.3. Electrophilic attack with electron abstraction**

388 In addition to the reductive capability from the surface-confined electron-rich EPFRs, Dong et al.
389 suggested that the EPFRs on dissolved organic matter (DOM) released from biochar matrices to bulk

390 solution exhibited pronounced oxidative ability towards As(III) on the basis of EPR technique.¹²⁴ Biochars
 391 developed from cow manure and rice husk at 300 or 700 °C were also reported to directly interact with 1,
 392 3-dichloropropene, and reached slow reaction constant of $k_{obs} = 0.35\text{--}1.47 \times 10^{-4} \text{ min}^{-1}$ but effective
 393 removal efficiencies (55–95.5 %). This phenomenon might be ascribed to the EPFRs decorated inside
 394 biochar slurry (biochar surface or released DOM).^{95, 129} Fang et al. further utilized PDS/biochar activation
 395 system for efficient remediation of polychlorinated biphenyl,⁸⁹ and found PDS activation was
 396 predominantly influenced by types and density of EPFRs, as evidenced by the linear correlations between
 397 the consumption of EPFRs and generated SO_4^- amount, or $\lambda = [\text{generated } \text{SO}_4^- \text{ amount}] / [\text{EPFRs}$
 398 $\text{consumption}]$ and g-factor. Several studies also reported the photoexcitation-induced electron transition
 399 regime in biochar, and deduced that the EPFRs over biochar surface or in DOM coupled with other
 400 quinone-like substances played key roles in producing $^1\text{O}_2$ for organics degradation, which is highly
 401 relevant to the aforementioned geobattery theory.¹³⁰ EPFRs-activated PDS systems on biochar were also
 402 applied in the soil remediation to efficiently degrade bisphenol A,¹³¹ providing a fascinating strategy for
 403 practical applications under different substrates. **Nevertheless, the environmental concern of EPFRs**
 404 **should be underlined in future study as they are defined as organic/metal nanoparticle pollutant.**

405 Overall, EPFRs formation and electrochemical behaviour are briefly depicted in **Fig. 5**. Accordingly,
 406 the possible reaction pathways during the EPFRs-induced peroxides activation could be proposed
 407 (exemplified by PDS/ BC_{EPFRs} , **Eqs.3-7**):



413 **Table 2** summarizes the catalytic performance of various electroactive components on biochar. With
414 respect to the reaction kinetics, carbocatalysis of EPFRs-based biochars shows trivial disparity from that
415 of functionalities-based biochars. Overall, RAMs-induced carbocatalysis requires relatively long reaction
416 time, which may imply the longstanding and mild electrochemical catalysis *via* RAMs on biochar.

417

418 **3. Metal incorporation for enhanced electron-transfer carbocatalysis on biochar**

419 **3.1. Characteristics of metal incorporated biochar**

420 **3.1.1. Synergies between carbon structure and metal sites**

421 Transition metals and their oxides can serve as widely distributed and easily accessible catalysts to
422 donate electrons for various catalytic processes, while the irrevocable deficiencies such as poor affinity
423 towards reactants (*i.e.*, peroxides or pollutants) due to their intrinsic surface chemistry (*i.e.*, low specific
424 surface area and pore volume, inherent surface energy, and unfavourable charged surface, *etc.*) and
425 detrimental leaching potential inhibit their wider application.⁸³ Using biochar as a carbon-based scaffold
426 to harbour metal active centres has been extensively applied in environmental remediation. Electron
427 mobility can be effectively improved by graphitic carbon framework and electron-rich sites are evenly
428 distributed over carbon to afford more accessible sites.¹⁸ Such a carbon/metal configuration can help to
429 alleviate the potential deactivation of carbon layer and strengthen affinity towards oxyanions with
430 improved surface characteristics.² More importantly, well-developed biochar matrices are conducive to
431 immobilizing active metal centres and efficiently reducing the metal leaching. Hence, this may allow for
432 scalable production of carbon-based catalysts with desirable electroactive sites.

433 **3.1.2 Improved physicochemical properties of biochar after metal incorporation**

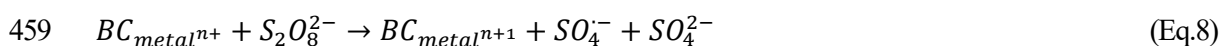
434 Previous research studying metal-incorporated biochars strived to reach practical objectives including:
435 (a) enhancing the separation and recyclability of biochar by endowing ferromagnetism to the metal-
436 biochar composites (*e.g.*, iron, cobalt, and nickel) after environmental applications in aqueous solution;

437 (b) promoting the adsorption capacity of raw biochars towards anionic metalloids or organic pollutants by
438 enhancing electrostatic affinity and surface complexation; and (c) acting as pore forming agents due to the
439 catalytic capability of metal centres (*i.e.*, as hot spots to catalyse reforming) under high temperature that
440 both inherent mineral ash and exterior metal contents can catalytically improve the textural characteristics
441 of biochar during thermochemical conversion.³⁴ It is noteworthy that although a wide array of studies has
442 been conducted, the intrinsic redox process on the solid-liquid interface of biochar received insufficient
443 emphasis on custom design of biochar production.⁸⁰

444 **3.1.3 Approaches to fabricate metal biochar with electroactive properties**

445 The incorporation of metal or metal oxides within biochar matrices can be achieved *via* two major ways:

446 (a) pre-mixing of metal salts with raw biomass through various mechanochemical processing methods
447 (wet impregnation, ball-milling, and dry agitation), followed by pyrolysis or hydrothermal carbonization
448 under predetermined conditions (*i.e.*, pre-synthesis medication); and (b) post-mixing of metal salts with
449 biochar containing abundant oxygen-containing functional groups to reach modulated physicochemical
450 properties after thermal treatment (*i.e.*, post-synthesis medication). The incorporation of metal
451 components inside biochars can adjust the surface chemistry of raw biochars and enable better
452 electrocatalysis during the charge-dominated processes.² Effective electron transfer from incorporated
453 metals to the conjugated carbon framework would increase the local electronic states of carbon surface at
454 localized region. Commonly incorporated metals on biochar include iron, copper, manganese, and
455 aluminium, *etc.*, while only several transition metal (*e.g.*, Fe and Cu) systems involve electron-mediated
456 efficacy and are critically emphasized in this review. The typical reaction pathway during the metal-
457 induced peroxides activation follows the Lewis acid/base pairs theory (as exemplified by PDS/BC_{metal},
458 **Eq.8**):



460 **3.2. Electroactive remediation with metal biochar**

461 **3.2.1. Direct electron donation by iron-based metal biochar**

462 High electron-donating capability of nanoscale zero-valent iron (nZVI) has been compatibly combined
463 with various support materials.¹³² Carbonaceous materials could serve as a porous support to disperse and
464 stabilize metal nanoparticles to facilitate their environmental applications. Using waste-derived biochar to
465 support nZVI particles is potentially more environmentally friendly and economically competitive. Zhou
466 et al. first adopted biochar as mechanical support to disperse and stabilize ZVI nano-particles to remediate
467 Pb(II), Cr(VI), As(V), phosphate (P), and methylene blue (MB) from aqueous solutions.¹³³ In recent years,
468 many nZVI-biochar focused on the efficient reducibility of ZVI while few research studies scrutinized the
469 synergistic effects among different components on biochar including metal contents, RAMs, and
470 graphitization framework, *etc.* Recently, Sun et al. fabricated a multifunctional ZVI/biochar derived from
471 two-step pyrolysis of FeCl₃-impregnated biochar (without the hazardous use of sodium borohydride as
472 reductant) and found that the reducibility of embedded metal nanoparticles could be considerably
473 enhanced with the highly conjugated carbon domain acting as electronic modifier.¹⁸ Moreover, iron oxides
474 are also found to be reductively potent when collaborating with RAMs on biochar. Zhong et al. reported
475 an enhanced Cr(VI) removal rate by a hybrid adsorption-reduction process using Fe₃O₄ acting as the
476 crucial redox sites on biochar, and EPFRs were verified to effectively participate within and induced an
477 indispensable synergistic effect with metal centres in Cr(VI) reduction.⁵⁶

478 **3.2.1. Mild and sustainable electrocatalysis with specified metal incorporation**

479 In addition to the most ubiquitous iron- and iron oxide-incorporated biochar, copper provides a unique
480 strategy for metal-biochar production with its mild catalytic features. As a low-toxicity, high-efficiency,
481 [abundantly](#) available, and stable mineral content, copper and its oxides (CuO and Cu₂O) arise as
482 promising candidates for wastewater treatment.¹³⁴ Zhong et al. prepared a N and Cu co-doped biochar for
483 oxidative degradation of tetracycline and showed that the incorporated copper particles could provide free
484 electrons to induce radical generation *via* plausible Cu²⁺/Cu³⁺ redox recycling in aqueous solution.¹³⁵

485 Since the discovery of efficient PMS activation by CuO *via* an appealing sustainable non-radical route,¹³⁶
486 many researchers have been devoted to exploiting this intriguing feature but most found it irreproducible.
487 It might result from the misapprehension to the role of CuO in non-radical activation. Recently, Zhu et al.
488 presented the non-radical PDS activation *via* ¹O₂ generation on crystallographic manganese oxides, which
489 was elaborated adopting sophisticated methodology (*i.e.*, EPR analysis, chemical probes, scavenger
490 experiments, and solvent shift) and deemed to originate from the metastable complexes formed on the
491 manganese surface.²¹ Wan et al. proved the formation of metastable oxyanion complexes on Cu species
492 which posed nonnegligible direct oxidative potential towards electron donors (*i.e.*, organic pollutants), and
493 the incorporation of Cu nanoparticles on biochar surface could benefit from the graphitic biochar structure
494 to induce remarkable ¹O₂ generation.⁵⁵ Compared with the nature of radical-based oxidation that radicals
495 will be generated spontaneously as long as catalyst and oxyanions are available independent of the
496 presence of target pollutants, the evolvement of non-radical pathway helps to preserve the excessive
497 oxyanion molecules once pollutants are depleted and avoid the unproductive oxidation towards carbon
498 surface. Additionally, the generated powerful radicals are usually accompanied with side effects like non-
499 selectivity (*i.e.*, depletion by water molecules, ease of being scavenged by natural organic matters, and
500 generation of highly halogenated products), while sustainable non-radical oxidation presents mild
501 reactivity and better selectivity to electron-rich pollutants. It is noteworthy that the vulnerability of the
502 organic pollutants toward nucleophilic attack from direct electron donation is generally determined by its
503 ionized potential and macromolecular functionality of the aromatic structure.¹³⁷

504 Irrespective of the non-radical activation potential, aforementioned Cu species as the *p*-type
505 semiconducting materials have a relatively narrow band gap of 1.8–2.2 eV and 1.2–1.8 eV, making these
506 materials promising in photoelectronic devices, sensors, and batteries industries.¹³⁸ Khataee et al.
507 synthesized a Cu₂O-CuO@biochar composite by hydrothermal procedure as an efficient photocatalyst
508 for photodecomposition of Reactive Orange 29, where photocatalytic performance of Cu₂O-CuO could

509 be enhanced upon carbon structure.¹³⁹ Similarly, a series of TiO₂/biochar composite catalysts were
510 prepared by Lu et al. for the photocatalytic degradation of methyl orange. Appropriate biochar ratio was
511 found to promote the activity of TiO₂ and increase decolorization and mineralization efficiency by 20.8%
512 and 51.0%, respectively, as compared to TiO₂ control group.⁶¹ Kim et al. used biochar as an economical
513 and effective support for TiO₂ to lower the recombination rate of free electrons and holes during
514 photocatalysis.¹⁴⁰ Lisowski et al. also reported the a superior photocatalytic ability of TiO₂/biochar with
515 reproducible high photocatalytic efficiency.¹⁴¹

516 **3.3. Bottlenecks of metal incorporated biochar**

517 For the present manganese-, cobalt-, or some bimetallic-biochar researches, the metal centres were
518 deployed merely as Lewis basic sites or electron donors during the electron-mediated processes, and redox
519 recycling potential were still poorly optimized.^{64, 142-147} More importantly, the ineluctable high toxicity
520 from secondary contamination violates with the principles of green chemistry and green engineering.
521 Sustainable countermeasures such as non-radical degradation should be further emphasized in the future.
522 It is well acknowledged that these metal/biochar composites possess high reactivity, but they are less
523 sustainable (poor reusability, metal leaching, and non-selectivity, *etc.*) as compared to non-carbon
524 heteroatoms doped biochar. Considering the inherent structural complexity of biochar matrices, metal
525 centres are required to be associated together with other biochar components rather than isolated and
526 analysed individually, especially on the rational redox reaction processes. Considering the current
527 bottleneck and imperative demand for sustainability [from the view of life cycle assessment](#), we propose
528 that the future directions should point to the metal-free heteroatoms doping technique.

529

530 **4. Defects engineering for promoted electron-transfer carbocatalysis on biochar**

531 **4.1. Intrinsic structural complexity and nonstoichiometric nature of biochar**

532 Electrochemical carbocatalysis intimately correlates with the intrinsic carbon configuration and
533 structural dimension of carbonaceous materials. The direct application of high-dimensional granular
534 carbonaceous materials including biochar, AC, and mesoporous carbon showed inferior catalytic
535 performance and poor stability in AOPs. The intrinsic structural complexity and nonstoichiometric nature
536 of carbon framework stemmed from diverse feedstocks hinder the rational exploration of their
537 mechanistic reaction routes. The active sites can be barely differentiated under varied conditions, and
538 carbocatalysis is usually governed by multiple constituents like RAMs, hexagonal units, porosity, and
539 intrinsic minerals simultaneously.² Formerly, low-dimensional carbonaceous materials such as various
540 noble nanocarbons were chosen as the simplified carbon-based models to probe the modification
541 strategies and underlying mechanisms of carbocatalysis, while the investigation into sole component on
542 carbon structure would result in the inevitable neglects towards the ubiquitous synergistic effects on high-
543 dimensional carbon structure.

544 **4.2. Important role of adsorption to electrochemical catalysis**

545 Molecular arrangement of carbon materials are typically associated with adsorption capacity towards
546 organic compounds, which sequentially follows 0D (fullerene and nanodiamonds) < 1D (single-walled
547 or multi-walled carbon nanotubes) < 2D (graphene and graphitic carbon nitride) < 3D (cubic mesoporous
548 carbon, AC, and biochar).¹ It is basically acknowledged that the adsorptive capacity of carbonaceous
549 materials originates from optimal porous structure and greater surface area for better anchoring of
550 adsorbates.

551 With respect to biochar, its adsorptive performance towards organic pollutants relies on electrostatic
552 force, hydrophobic interaction, pore-filling adsorption/partition coupled with π - π interaction, and
553 chemisorption with hydrogen bonding, while its adsorptive behaviour towards metals/metalloids is
554 determined by chemical (co-)precipitation, ion exchange, and complexation with surface functional
555 groups. Although adsorption is not an electron transfer process, the enrichment of pollutant molecules

556 around the active sites is beneficial to the redox reactions afterwards. The evolution of rich porous structure
557 in biochar can notably increase its carbocatalysis because mesoporous can facilitate mass transfer and
558 subsequent adsorption for better reactant/substrate contact. Considering the cost-effectiveness and strong
559 adsorption capacity of biochar in contrast to expensive low-dimensional nanocarbons, biochars have
560 manifested their promising prospect as easily manoeuvrable structural constitutes to reach an enhanced
561 dual-function of adsorption and carbocatalysis.

562 4.2. Nonnegligible electrocatalysis from defective sites

563 Since Wang et al. reported the superior catalytic performance of various nanocarbons, which primarily
564 stemmed from the open sp^2 -hybridized carbon matrices with rich zigzag/armchain edges and vacancy
565 defects,¹ structural engineering with reactive defective sites has been an emerging technique applied in
566 carbon-involved environmental field. The electrochemically reactive zigzag edges on rGO were first
567 observed to simulate PMS to generate $SO_4^{\cdot-}$ for the remediation of phenolics.¹¹³ Then, Duan et al. further
568 investigated the critical active sites in graphene-catalysed PMS activation system, and a positive
569 correlation was put forward between reaction rate constant and defective level. Calcinating temperature
570 was adopted to readily regulate degrees of defects within carbon lattice.⁵⁷ Furthermore, theoretical
571 calculation suggested that edge defects and vacancy defects are much more reactive than graphitic
572 honeycomb basal plane to bind with oxyanions with the help of DFT modelling.^{57, 121} Zigzag/armchain
573 defects are able to cleave peroxide O-O bond *via* direct electron donation, while vacancies appear to be
574 capable of harbouring oxyanion molecules to form a oxyanion-carbon complexes *via* a non-radical
575 route.¹⁴⁸ Besides, micropores are also considered as point defects and active sites conducive to
576 carbocatalysis. Numerous publications on relevant carbon-based materials have already emphasized the
577 indispensable impacts of high curvature regions (or highly strained regions), pentagon defects, edges, and
578 vacancies in the carbocatalysis.¹⁴⁹ As the electron-rich carbon species along the carbon matrix peripheries
579 are expected to play an important role in this electron transition process, better control in the microstructure

580 morphology and appropriate population of structural defects should be further customised on biochar
581 design.

582 **4.3. Optimization and implementation of defective sites on biochar**

583 Inspired by the cutting-edge progress on nanocarbons, structural engineering on biochar has started to
584 drive growing research. Typically, Zhu et al. managed to fabricate a highly graphitized biochar with
585 tailored defective degree under 900 °C pyrolysis. This work revealed the reinforced adsorption capacity
586 towards reactants associated with greater defective level could accelerate the formation of electrophilic
587 oxyanion-carbon complexes oxidative to pollutants.³⁶ Another non-radical electron-involved PDS
588 activation based on singlet oxygenation was subsequently proposed for biochar after CO₂ activation under
589 800–950 °C to create a richer defective structure.¹¹⁶ The generation of different reactive species might
590 come from their distinct coupled modification technique and parent precursors. Meanwhile, Liang et al.
591 carefully compared the differences between biochar and AC for persulfate activation, evidencing the
592 higher defective sites would transform the dominance of released radicals in bulk solution into solid-phase
593 type radicals with a specific sequence as BC400 (radicals mostly released in solution, low defect level),
594 BC700 (radicals partially in solid phase, medium defect level), and AC (radicals mainly in solid phase,
595 high defect level).¹⁵⁰ The radical-based scenario was also supported by Ouyang et al., as biochar derived
596 from pine needles under 800 °C with abundant micropores and defective structures contributed to the
597 generation of SO₄^{•-} and [•]OH in PMS activation with a single-electron transfer process.¹⁵¹ Similarly, lignin-
598 based biochar pyrolyzed at 720 °C under CO₂ medium was found to be reactive to induce the generation
599 of SO₄^{•-} *via* direct one-electron transfer from biochar to PDS molecules.⁶⁴ Herein, typical electrochemical
600 interactions with defective sites are described in **Fig. 6**.

601 **4.4. Present progress of defects engineering on biochar**

602 Overall, the defects engineering on biochars is still limited at the present stage and most of the relevant
603 studies emphasized the synergistic effects of defective sites coupled with other components such as RAMs

604 and doped heteroatoms with edge sites as ideal anchoring points. This may suggest that the free-flowing
605 electrons on biochar boundaries are still severely confined in geometry and scarce in quantity. Defects
606 along the carbon species highly rely on the well-developed micropore structure and distorted graphite
607 units, which are susceptible to erosive surface oxidation from the generated ROS. Besides, pyrolytic
608 temperature and oxygen level also exert critical impacts on the electrocatalytic performance of various
609 defects, which impede their fabrication and optimization. In terms of pristine biochar nature, higher
610 temperature coupled with specified processing methods (CO₂ purging, alkaline activation, and acidic
611 treatment, *etc.*) are generally regarded as the efficient manners to tailor the defective level of biochar.
612 Nevertheless, excessive increase of defective level is not recommended because this will influence the
613 structural integrity and reduce the mechanical strength of biochar framework.

614

615 **5. Non-metal heteroatoms doping for distinct electron-transfer carbocatalysis on biochars**

616 **5.1. Heteroatoms doping turns ‘inert’ into ‘active’**

617 Heteroatoms doping technique with noncarbon atoms including N, B, and S, *etc.* [has been widely](#)
618 applied to synthesize functionalized carbonaceous materials, especially on well-ordered crystalline carbon
619 network, to obtain modulated physicochemical properties.^{152, 153} Although introducing various noncarbon
620 heteroatoms within the crystalline network could be classified as feasible methods to create point defects,
621 the heteroatoms doping is recommended to be categorized individually from defects engineering in the
622 electrocatalytic processes in view of its unique electroactive performance. In principle, defects could be
623 regarded as topological deviations of pristine graphitic carbon network such as alien components-induced
624 pentagons/heptagons formation, while heteroatoms doping would endow a disrupted electronic culture to
625 pristine carbon matrices. The incorporated foreign heteroatoms possess distinct electronegativity, electron
626 density, and atomic radius/orbitals, so that it could turn chemically inert carbon framework into reactive
627 state by disrupting the electrochemical and spin culture of original *sp*²-hybridized carbon.² For ubiquitous

628 heteroatoms doping on crystalline carbon, the single-element doping of B, P, or I was found to be
629 ineffective for simplified carbon model scaffold like graphene in environmental applications,¹⁵⁴ whereas
630 N doping was reported to be highly reactive in redox reactions with a good catalytic performance of N-
631 functionalized carbonaceous materials in AOPs and biorefinery reactions.¹⁵⁵

632 **5.2. Versatile impacts from nitrogen dopants**

633 As typical basic sites, various N dopants have been deployed on biochar matrices to enrich its surface
634 adsorptive sites and/or introduce more positive charges to modify biochar surface.¹⁵⁶ The chemical
635 complexation affinity with soft to borderline metals (*e.g.*, Cu, Pb, and Cd), adsorptive affinity towards
636 acidic gas pollutants (*e.g.*, CO₂ and SO₂), and electrostatic force towards anionic pollutants could be
637 significantly enhanced after N functionalization. For instance, Xu et al. employed a facile ball-milling
638 method to successfully dope N basic sites on the inert and negatively charged surface of pristine biochar
639 (450 °C) using kinetic energy of moving balls, by which CO₂ uptake and reactive red removal were
640 significantly enhanced afterwards.¹⁵⁷

641 Electroactive N dopants incorporate three classes, *i.e.*, pyridinic N (N dopant in 6-membered
642 heteroring), pyrrolic N (N dopant in 5-membered heteroring), and graphitic N (namely quaternary N, *sp*²-
643 hybridized N adjacent to three *sp*² carbon atoms), and the introduction of N dopants is chemically different
644 from aminated modification with amino/oxynitride groups linked on the carbon boundaries. Compared
645 to RAMs mainly bound/extended along the peripheries of carbon species, the incorporated alien N atoms
646 act as substitutes to carbon atoms in ordered carbon units to form heteroring at atomic scale.¹⁴⁹ The
647 incorporation of N heteroatoms with higher nucleophilic nature is expected to reinforce the resistance of
648 pristine biochar structure towards surface oxidation reaction, thus promising better recyclability and long-
649 term operational potential.¹¹⁵

650 **5.3. Electroactive properties of respective nitrogen dopant**

651 Respective N dopant configuration displays different electronic properties as well, as pyridinic N and
652 pyrrolic N are relatively less effective to mediate electron transition.¹⁵⁸ The sp^2 -hybridized graphitic N
653 possesses unpaired electrons with paramagnetic properties, forming delocalized conjugated π system
654 within carbon framework, and the high electronegativity (Pauling scale $\chi_n = 3.04$) enables graphitic N
655 atom to abstract electrons from adjacent carbon (Pauling scale $\chi_c = 2.55$) and alter the electron density in
656 a localized region of carbon framework. According to approximate calculation, each graphitic N can add
657 ~ 0.5 free electron to the carbon π -network, while pyridinic N and nitrile N remove charges from carbon
658 structure to form p -type doping. Meanwhile, the graphitic N in carbon lattice could decrease the
659 dissociation energy barrier of absorbed oxygen species,¹⁴⁹ which is expected to account for the sustainable
660 oxygen species activation. Hence, graphitic N appears to be more ideal for electron-mediated processes
661 like AOPs. Thus, graphitic N is regarded as the desired N dopant configuration for biochar-based
662 carbocatalysis, though it is still not clear which one of these two typical graphitic N configurations, namely
663 valley-type and centre-type graphitic N species, should be responsible for the catalytic performance.¹⁵⁹
664 Thermal treatment over 500 °C under inert atmosphere is regarded as facile method to screen other N
665 configurations on carbon surface because graphitic N is more thermally stable and relatively difficult to
666 decompose, leading to a larger proportion of graphitic N in the resultant biochar samples.^{36, 115}

667 **5.4. Enhanced electroactivity of biochar from heteroatom doping technique**

668 **5.4.1 Heteroatom doping from raw biomass**

669 With respect to N-doping technique for biochar, N source could originate from raw biomass itself or
670 external introduction from accompanied N-rich precursors or purging ammonium gas, generating varied
671 N-doping categories on biochar. For instance, Rong et al. utilized banana peels as composite biochar
672 precursor and N source to synthesize magnetic N-doped biochar *via* a facile one-pot thermal process. The
673 resultant biochar was used as the cost-effective and recyclable electron donor for PDS activation.¹⁶⁰
674 Similarly, Ho et al. fabricated a novel N-doped biochar from direct pyrolysis of C-phycocyanin extracted

675 *Spirulina* residue, and the self-doping of graphitic N could be achieved under high pyrolytic temperature
676 (900 °C) from the inherent protein contents in algae for efficient electron transfer to PDS molecules.³⁴ A
677 human-hair-derived N, S-doped porous biochar was also successfully fabricated under high temperature
678 (800 °C), and outperformed most traditional metal-based catalysts towards PMS activation for bisphenol
679 A degradation, wherein the incorporated graphitic N exhibited good function to circulate electron flow
680 and adjust the electron density of adjacent carbon atoms.¹⁶¹ It is noteworthy that the slight doping of S
681 contents (1.04 at. %), mainly consisting of thiophene S on the edge sites rather than inert oxygenated S,
682 was also emphasized in this research as co-doping agent to enhance electrochemical carbocatalysis.

683 Different from B (Pauling scale $\chi_B = 2.05$) and N atoms, S atoms (Pauling scale $\chi_S = 2.58$) display a
684 similar electronegativity to that of carbon atoms.¹⁴⁹ Hence, the secondary S dopant tends to act as spin-
685 dominated heteroatoms to disrupt the spin nature of carbon matrices, resulting in a more intimately
686 interactive surface with oxyanions to decrease the energy barrier of peroxide bond for electron
687 stimulation.¹⁶² Besides, the co-doping technology could enormously enlarge the positively charged region
688 through synergistic effects, which favours to provide more exposed active sites for promoted dual-
689 function of adsorption and carbocatalysis.¹⁴⁸ Meanwhile, excessive S doping would inflict a negative
690 effect on the redox reaction, resulting from the chaotic redistribution of unconfined electrons/spins and
691 disbalanced π system¹⁶³. Electrochemical interactions with heteroatoms doping as the critical
692 electroactive components are illustrated in **Fig. 6**.

693 **5.4.2 Heteroatom doping induced by exterior chemical modifiers**

694 As for external N-source doping on raw biomass *via* thermal treatment, the common nitrogen additives
695 include organic type (*i.e.*, urea and melamine) and inorganic ones (*i.e.*, ammonium salts and ammonia).
696 Recently, N-doped graphitic biochar derived from co-pyrolysis of reed mixed with urea under 900 °C
697 displayed an increased graphitic N level to enhance the non-radical activation of PDS *via* a two-electron
698 process.³⁶ Nevertheless, opposite findings were observed that urea-derived N functionalization for biochar

699 led to preferential introduction of pyrrolic N and pyridinic N while no regularity was found for graphitic
700 N.³⁵ The edge-nitrogenated biochar functionalized with large amount of pyrrolic N and pyridinic N was
701 able to evolve the formation of surface-bound reactive PDS complexes followed with a direct electron
702 abstraction process to degrade pollutants. This contradictory scenario indicates that the N doping
703 technology on biochar structure is still in its infancy stage, and future work should focus on the
704 investigation of the stoichiometric type of electroactive N dopants and the customisation of yield and
705 density.

706 **5.5. Future direction of electroactive heteroatom doping on biochar**

707 In consideration of the associated environmental impacts of nitrous oxide as greenhouse gas emissions,
708 inorganic nitrogen precursors (*i.e.*, NH₄Cl and NH₃) are less explored, and usually utilized as pore volume
709 and surface area improving agents under pyrolytic temperature. Carbocatalysis from tuneable electronic
710 features by the formed carbon-noncarbon heteroring is usually neglected in these processes. For instance,
711 Lian et al. manufactured a N-doped microporous biochar from crop straws pyrolyzed at 800 °C with
712 ammonia purging for 3 h, which exhibited high micropore volume (71.5%) and nitrogen content (8.81
713 at. %). The N dopants [generated under NH₃ purging](#) were only employed as basic sites for [the adsorption](#)
714 [of anionic dye molecules](#).¹⁶⁴ [Their electroactive properties are recommended to be further addressed as](#)
715 [Mian et al. fabricated a magnetic N-doped biochar under similar operational conditions \(800 °C with](#)
716 [ammonia purging\) and found those introduced nitrogen dopants caused the reduction of Cr\(VI\) into](#)
717 [Cr\(III\)](#).¹⁶⁵ In addition, a P-doped biochar prepared from corn straw by one-step manufacture might possess
718 high electroactive capability owing to the lower electronegativity of P and larger covalent radius, but it
719 was solely elucidated into its adsorption behaviour rather than electron-mediated carbocatalysis.¹⁶⁶

720 Apart from insufficient understanding on N-functionalized biochars, B, S, P, and other co-doping
721 technologies applied on biochar matrices also need further exploration. Currently, they are restrained by
722 the critical demands in fabrication technique for well-ordered carbon π -system and favourable edge sites

723 to accomplish efficient doping of heteroatoms dopants. The autonomous doping using contents
724 comprising of N, S, and B, *etc.* in raw biomass waste without extra additives should be more desirable in
725 line with economical and facile-production nature of biochar. It should be noted that when specific
726 applications require drastic and fast electron activities, metal-incorporated biochar is more desirable, while
727 metal-free heteroatoms doped biochar is recommended for mild reactions owing to its high sustainability.
728 Furthermore, the synergistic effects originated from heteroatoms should receive a greater emphasis,
729 because heteroatoms are prone to locate at edge sites and give rise to the distortion of carbon lattice to
730 generate defective sites. This requires more sophisticated protocols (yet practical and scalable) based on
731 new insights and holistic understanding of both defects engineering and surface heteroatoms modification
732 towards the roles of molecular structures on biochar.

733

734 **6. Conductive surface for expedited electron flowing on biochar**

735 **6.1. Electron transfer *via* conductive surface of ordered carbon lattice**

736 Lately, well-ordered carbon matrices are found to pose distinct electronic properties to serve as efficient
737 electron shuttles, deliver charges among aromatic units, and prompt inherent catalytic redox reactions on
738 the surface of carbonaceous materials.^{25, 167} For instance, various carbonaceous materials (graphene, black
739 carbon, and biochar, *etc.*) could act as electron transfer mediators in biotic redox behaviour.¹⁶⁸⁻¹⁷⁰ Biochar
740 addition could also promote direct interspecies electron transfer (DIET) and improve biogas production
741 in anaerobic digestion.^{171, 172} This appealing phenomenon is closely associated with the synergies among
742 electron-rich RAMs, incorporated metals/oxides, various defective sites, doped heteroatoms, and sp^2 -
743 hybridized conjugated carbon π -network. Previously, nanodiamonds that possesses a sp^3 -hybridized core
744 and coated with amorphous carbon layer were found to be ineffective for electron abstraction in PDS
745 activation, while rGO-900 with sp^2 -hybridized lattices and plentiful defective sites, non-hexagonal units,
746 and RAMs demonstrated **superior** electroactive performance for catalytic reactions.¹ Lee et al. further

747 verified that partially graphitized nanodiamond composed of a sp^3 -hybridized core surrounded by sp^2 -
748 hybridized carbon layer exhibited excellent electrocatalysis compared with inert pristine nanodiamond,
749 confirming the critical role of conjugated carbon units.²⁴ As an intact, ordered, and electrophilic matrix,
750 graphitic carbon lattice within carbonaceous materials could deliver electron flows from electron donors
751 (*i.e.*, organic pollutants and multivalent metals/metalloids) to electron acceptors (*i.e.*, oxyanions or free O_2
752 molecules) *via* the conductive carbon surface owing to the differences of their redox potentials as inherent
753 driving force. Nonetheless, the highly conductive graphitic carbonaceous interfaces such as fullerene and
754 graphitic carbon nitride were ineffective to initiate the electron-based carbocatalysis,¹ suggesting that
755 electron transition *via* graphitic lattice should be encouraged by multilateral causes rather than solely by
756 conjugated carbon π -network.

757 **6.2. The proposal of geobattery theory on biochar**

758 As an integrated carbonaceous structure consisting of crosslinked sp^3 -hybridized, sp^2 -hybridized, and
759 amorphous carbon atoms with massive electroactive defects and RAMs on the surface, biochar is
760 expected to trigger extraordinary electroactive carbocatalysis with its scalable surface chemistry and
761 versatile structural arrangement. Accompanied with geobattery theory proposed by Sun et al. on natural
762 pyrogenic carbon, geoconductor theory (electron shuttle *via* conductive carbon substrate) has recently
763 been demonstrated on engineered biochar in environmental applications.¹⁰⁵ Yu et al. proposed a top-down
764 methodology to differentiate the individual role of different components on sludge-derived biochars, in
765 which graphitic carbon matrix primarily took over when pyrolytic temperature was elevated to 800 °C,
766 while the acid-soluble substances should account for charge-dominated behaviour of biochar pyrolyzed
767 at 400 and 600 °C.¹⁷³ This suggests the crucial properties of sp^2 -hybridized graphitic carbon on electron
768 transfer regime. Wan et al. found that the biochar structure appeared to conduct the free-flowing electrons
769 from the entrapped ZVI to exterior electron acceptor (*i.e.*, Cr(VI)) *via* micro-electrolysis process. Owing
770 to the inherent difference of redox potential between Fe^0 and Cr(VI), the free electrons entrapped within

771 the hierarchical structure could be excited to transfer outwards along the conjugated carbon units.²³ Peanut
772 shell-derived biochar pyrolyzed at 700 °C could also act as electron shuttle in redox reactions, where
773 biochar accepted electrons from low molecular weight organic acids (LMWOAs) and then transferred
774 them to the electron acceptors, *e.g.*, Cr(VI).¹⁷⁴ Similarly, another low-temperature peanut shell-derived
775 biochar was found to potentially act as concurrent electron donor and shuttle for the reduction of Cr(VI)
776 with the help of various RAMs.¹⁷⁵

777 **6.3. Sustainable and green features of biochar electron shuttle**

778 The electron-shuttle scenario reflects the electrochemical properties of biochar, which further proves
779 the superior electron accepting capacity (EAC) and electron donating capacity (EDC) from the *sp*²-
780 hybridized graphitic carbon lattice.²⁷ These appealing electronic capacities are usually correlated with
781 sustainable non-radical species like singlet oxygenation, surface-confined reactive complexes or other
782 surface-bound ROS susceptible to electron-rich donors and show a better selectivity to electron-rich
783 pollutant. Usually, these sustainable non-radical behaviours take place as inherent surface chemical
784 reactions on carbon lattices, and refer to green and mild pathways without relying on non-selective radicals
785 released into bulk solution. For instance, readily generated surface-bound reactive radicals were
786 considered to be responsible for PDS activation utilizing graphitic wood-derived biochar pyrolyzed at
787 700 °C, and the RAMs including EPFRs and C–OH on graphitized carbon structure accounted for
788 confined-radical generation.¹¹² The aforementioned copper incorporated graphitic biochar was found to
789 initiate the generation of ¹O₂ derived from surface reactive complexes attached on copper atoms and
790 accept the unconfined electrons transferred from organic pollutants *via* graphitic carbon matrices.⁵⁵ The
791 comparison between AC and biochar pyrolyzed at 700 °C with respect to the generation of solid-confined
792 radicals unveiled the synergies between defective sites and carbon matrices.¹⁵⁰ Irrespective of the specific
793 N dopants, both the edge-nitrogenated (pyrrolic N and pyridinic N) biochar and the N-doped biochar
794 functionalized with graphitic N were testified to prompt the generation of surface-bound reactive

795 complexes that subsequently attacked organic pollutants *via* a direct electron transfer regime along the
796 graphitic carbon lattice.^{34,35} It appears the highly order sp^2 -hybridised carbon structure can act as excellent
797 enhancer or bridge to synergize with the electrochemical behaviours from other components on biochar,
798 and account for especially direct electron transfer. Specifically, the non-radical catalytic reaction is first
799 initiated by electroactive sites like RAMs, metal active sites, and defective sites to trigger electron flow by
800 an electrochemical force from geobattery pairs, then the prompted unconfined electrons could migrate
801 along the conjugated biochar matrices with abundant π -electrons acting as a geoconductor/shuttle. The
802 typical electrons migration behaviour on conductive biochar matrices is illustrated in **Fig. 7**.

803 Overall, the conductive conjugated carbon surface of properly engineered biochar poses the potential
804 to evolve green and sustainable remediation of electron-rich pollutants. The graphitic carbon structure,
805 surface chemistry, and the customisation of inherent synergistic effects are of great significance to foster
806 sustainable development and wide applications, while the fabrication of biochar with **outstanding**
807 electrocatalysis still requires rational manipulation from both structural and chemical aspects in future
808 studies.

809

810 **7. Characterization and optimization of electroactive components on biochars**

811 For electroactive components on biochar, it is crucial to employ proper types of characterization
812 methods to explore their chemical properties and micro-scale morphology using both theoretical and
813 quantitative methods. From the perspectives on biochar characterization, X-ray diffraction (XRD,
814 crystalline and interlayer spacing), Fourier transform infrared spectrometry (FTIR, functionalities), X-ray
815 photoelectron spectroscopy (XPS, surface compositions and chemical states within a depth of < 10 nm),
816 Raman spectroscopy (defective and graphitic bands as indicative of carbon arrangement), elemental
817 analyser (EA, ultimate elemental analysis), scanning electron microscopy (SEM, surface morphological
818 images) coupled with X-ray dispersive spectroscopy (EDS, proximate elemental analysis), and

819 transmission electron microscopy (TEM, high-resolution morphology, pore diameter determination, and
820 crystalline spacing) associated with electron energy loss spectroscopy (EELS, valence mapping) are
821 mature techniques for characterizing biochars. Linear-sweep voltammograms (LSV) and [electrochemical](#)
822 impedance spectroscopic analysis (EIS) are also available techniques to probe the electron-shuttling
823 mechanism, charge transfer, and ion diffusion processes in electrode materials, respectively. Extended X-
824 Ray absorption fine structure (EXAFS) can help to characterize the polyaromatic structure of biochar with
825 multiple scattering resonance. Solid-state nuclear magnetic resonance (NMR) is able to determine the
826 carbon aromaticity and the content of protonated or non-protonated carbon atoms in biochars by Zeeman
827 splitting of spin level of nucleus under external magnetic field.⁸⁰ Electron paramagnetic resonance (EPR)
828 can help to qualitatively verify the RAMs type on biochars and quantitatively measure ROS intensity with
829 the addition of different spin trapping agents including 5,5-dimethyl-1-pyrroline N-oxide (DMPO) or
830 2,2,6,6-tetramethyl-4-piperidone (TEMP). Noteworthy, FTIR, XPS, XRD, LSV, and EA are important
831 characterization methods to determine oxygen functionalities and thus are recommended to quantitatively
832 verify the involvement of geobattery theory. Correspondingly, XPS, Raman, TEM, and EIS can
833 effectively indicate the graphitization of biochar and more suitable to illustrate electrochemical behaviour
834 following geoconductor theory.

835 Electroactive components can determine the inherent catalytic capability of biochar. Content levels and
836 species of respective components in the engineered biochar should be carefully customised in both
837 qualitative and quantitative manners. Adequate enrichment of electroactive components on biochar by
838 various processing methods involves chemical treatment (*e.g.*, acidic treatment, alkaline treatment,
839 oxidation modification, and metal salts/oxides modification) and physical treatment (*e.g.*, ball milling,
840 nanocarbons decoration, organic solvents etching, gas purging, and CO₂/steam activation). The target
841 electroactive components with modulated characteristics are summarized in **Table 3**. Besides, advanced

842 experimental and methodological methods to verify the role of electroactive component on biochars are
843 summarized in **Table 4** based on the latest cutting-edge research investigations.

844

845 **8. Conclusions and outlook**

846 Biochar has demonstrated its promising prospect as a cost-effective, environmentally benign, green,
847 and sustainable carbonaceous catalyst owing to its tuneable electroactive components for environmental
848 remediation. This emerging carbon-based redox system, as compared to nanocarbons with high
849 production cost or transition metals with toxic leaching potential, avoids the undesirable complicated
850 fabrication process with chemical- and energy-intensive input and detrimental secondary contamination.
851 With integrated fabrication-modification process and theoretical calculation for tailored electronic
852 properties of biochar, a comprehensive understanding of electrochemical carbocatalysis for biochar can
853 be achieved without compromising catalytic efficacy. Compared with RAMs or metal contents that are
854 irreversibly consumable, environmentally unstable under natural conditions, and even potential to cause
855 secondary contamination, the metal-free techniques (*e.g.*, non-carbon heteroatoms doping) can greatly
856 improve the inert and nonstoichiometric nature of engineered biochar, thus prompting versatile synergies
857 among different electroactive components to evolve non-radical reactive species, which should be
858 particularly highlighted to boost the progress of biochar-based redox carbocatalysis.

859 For directions of future research, rational manipulation of biochar graphitization, defective degree, and
860 carbon surface chemistry associated with functionalities within the tuneable biochar framework is
861 preferable to accomplish superior electroactive performance and good sustainability. Various advanced
862 methodologies and state-of-the-art surface characterization can serve to probe into the mechanistic routes.
863 While theoretical calculations *via* DFT have emerged as a computational tool to identify the roles of
864 different functionalities, defective sites, heteroatoms, carbon configurations, and the underlying
865 synergistic behaviour at the molecular level, an in-depth understanding of the origins to these

866 electrochemical processes on biochar should be further supported by more accurate and appropriate model
867 development. The appealing electrochemical processes without relying on non-selective ROS bring about
868 a new era, in which biochar can be tailored as green and sustainable metal-free catalysts in long-term
869 operation and mineralization of pollutants in natural medium in the presence of radical quenchers (*i.e.*,
870 inorganic ions and natural organic matter). We expect more studies from the research community to
871 capitalize on electrochemical aspects of engineered biochar in different fields (electrode materials, energy
872 conversion and storage, and supercapacitor, *etc.*) in addition to green and environmental remediation,
873 encouraging novel biochar-based systems for sustainable carbocatalysis in the future.

874

875 **Acknowledgements**

876 The authors appreciate the financial support from the Hong Kong Research Grants Council (PolyU
877 15217818) and Hong Kong International Airport Environment Fund (Phase 2) for this study.

878

879 **References**

- 880 1. X. Duan, H. Sun, K. Jian, Y. Wang and S. Wang, *Acs Catalysis*, 2015, **5**, 4629-4636.
- 881 2. X. Duan, H. Sun and S. Wang, *Accounts of Chemical Research*, 2018, **51**, 678.
- 882 3. P. R. Shukla, S. Wang, H. Sun, H. M. Ang and M. Tadé, *Applied Catalysis B: Environmental*, 2010,
883 **100**, 529-534.
- 884 4. W. Peng, S. Liu, H. Sun, Y. Yao, L. Zhi and S. Wang, *Journal of Materials Chemistry A*, 2013, **1**,
885 5854-5859.
- 886 5. I. Anastopoulos, I. Pashalidis, A. Hosseini-Bandegharaei, D. A. Giannakoudakis, A. Robalds, M.
887 Usman, L. B. Escudero, Y. Zhou, J. C. Colmenares, A. Núñez-Delgado and É. C. Lima, *Journal of*
888 *Molecular Liquids*, 2019, **295**, 111684.

- 889 6. J. C. Yoo, J. Beiyuan, L. Wang, T. Dcw, K. Baek, N. S. Bolan, Y. S. Ok and X. D. Li, *Science of the*
890 *Total Environment*, 2018, **616**.
- 891 7. J. Beiyuan, Y. M. Awad, F. Beckers, D. C. W. Tsang, Y. S. Ok and J. Rinklebe, *Chemosphere*, 2017,
892 **178**, 110-118.
- 893 8. A. D. Igalavithana, S. E. Lee, Y. H. Lee, T. Dcw, J. Rinklebe, E. E. Kwon and Y. S. Ok, *Chemosphere*,
894 2017, **174**, 593-603.
- 895 9. J. Sun, L. Pan, Y. Zhan, H. Lu, D. C. W. Tsang, W. Liu, X. Wang, X. Li and L. Zhu, *Science of the*
896 *Total Environment*, 2016, **544**, 670-676.
- 897 10. X. Yang, A. D. Igalavithana, S. E. Oh, H. Nam, M. Zhang, C. H. Wang, E. E. Kwon, D. C. W. Tsang
898 and Y. S. Ok, *The Science of the total environment*, 2018, **640-641**, 704-713.
- 899 11. C. Xinde, M. Lena, L. Yuan, G. Bin and H. Willie, *Environmental science & technology*, 2011, **45**,
900 4884-4889.
- 901 12. F. Yang, L. Zhao, B. Gao, X. Xu and X. Cao, *Environmental science & technology*, 2016, **50**, 2264-
902 2271.
- 903 13. J. J. Manyà, *Environmental science & technology*, 2012, **46**, 7939.
- 904 14. M. Inyang, B. Gao, Y. Ying, Y. Xue, A. R. Zimmerman, P. Pullammanappallil and X. Cao,
905 *Bioresource technology*, 2012, **110**, 50-56.
- 906 15. H. Peng, P. Gao, G. Chu, B. Pan, J. Peng and B. Xing, *Environ Pollut*, 2017, **229**, 846-853.
- 907 16. K. A. Thompson, K. K. Shimabuku, J. P. Kearns, D. R. U. Knappe, R. S. Summers and S. M. Cook,
908 *Environmental science & technology*, 2016, **50**, 11253-11262.
- 909 17. K. Vikrant, K. H. Kim, Y. S. Ok, T. Dcw, Y. F. Tsang, B. S. Giri and R. S. Singh, *Science of the Total*
910 *Environment*, 2017, **616-617**, 1242.
- 911 18. Y. Sun, I. K. M. Yu, D. C. W. Tsang, X. Cao, D. Lin, L. Wang, N. J. D. Graham, D. S. Alessi, M.
912 Komárek, Y. S. Ok, Y. Feng and X.-D. Li, *Environment International*, 2019, **124**, 521-532.

- 913 19. A. U. Rajapaksha, M. S. Alam, N. Chen, D. S. Alessi, A. D. Igalavithana, D. C. W. Tsang and S. O.
914 Yong, *Science of the Total Environment*, 2018, **625**.
- 915 20. X. Duan, H. Sun, M. Tade and S. Wang, *Catalysis Today*, 2018, **307**, 140-146.
- 916 21. S. Zhu, X. Li, J. Kang, X. Duan and S. Wang, *Environmental science & technology*, 2019, **53**, 307-
917 315.
- 918 22. D.-W. Cho, G. Kwon, K. Yoon, Y. F. Tsang, Y. S. Ok, E. E. Kwon and H. Song, *Energy Conversion
919 and Management*, 2017, **145**, 1-9.
- 920 23. Z. Wan, D.-W. Cho, D. C. W. Tsang, M. Li, T. Sun and F. Verpoort, *Environmental Pollution*, 2019,
921 **247**, 410-420.
- 922 24. H. Lee, H. I. Kim, S. Weon, W. Choi, Y. S. Hwang, J. Seo, C. Lee and J. H. Kim, *Environmental
923 science & technology*, 2016, **50**, 10134.
- 924 25. E. T. Yun, J. H. Lee, J. Kim, H. D. Park and J. Lee, *Environmental science & technology*, 2018, **52**,
925 7032-7042.
- 926 26. Y. S. Ok, S. X. Chang, B. Gao and H.-J. Chung, *Environmental Technology & Innovation*, 2015, **4**,
927 206-209.
- 928 27. Y. Yuan, N. Bolan, A. PrévotEAU, M. Vithanage, J. K. Biswas, Y. S. Ok and H. Wang, *Bioresource
929 technology*, 2017, **246**, 271-281.
- 930 28. I. K. M. Yu, X. Xiong, D. C. W. Tsang, Y. H. Ng, J. H. Clark, J. Fan, S. Zhang, C. Hu and Y. S. Ok,
931 *Green Chemistry*, 2019, **21**, 4341-4353.
- 932 29. G. Xue, Q. Wang, Y. Qian, P. Gao, Y. Su, Z. Liu, H. Chen, X. Li and J. Chen, *Journal of hazardous
933 materials*, 2019, **368**, 840-848.
- 934 30. K. Zhu, C. Jin, C. Zhao, R. Hu, Z. Klencsár, G. Ayyakannu Sundaram, D. F. Srankó, R. Ge and J.
935 Wang, *Chemical Engineering Journal*, 2019, **359**, 1537-1549.

- 936 31. H.-W. Man, C.-S. Tsang, M. M.-J. Li, J. Mo, B. Huang, L. Y. S. Lee, Y.-c. Leung, K.-Y. Wong and S.
937 C. E. Tsang, *Applied Catalysis B: Environmental*, 2019, **242**, 186-193.
- 938 32. R. Yin, W. Guo, H. Wang, J. Du, Q. Wu, J.-S. Chang and N. Ren, *Chemical Engineering Journal*,
939 2019, **357**, 589-599.
- 940 33. X. Cheng, H. Guo, Y. Zhang, Y. Liu, H. Liu and Y. Yang, *Journal of colloid and interface science*,
941 2016, **469**, 277-286.
- 942 34. S.-H. Ho, Y.-d. Chen, R. Li, C. Zhang, Y. Ge, G. Cao, M. Ma, X. Duan, S. Wang and N.-q. Ren,
943 *Water research*, 2019, **159**, 77-86.
- 944 35. H. Wang, W. Guo, B. Liu, Q. Wu, H. Luo, Q. Zhao, Q. Si, F. Sseguya and N. Ren, *Water research*,
945 2019, **160**, 405-414.
- 946 36. S. Zhu, X. Huang, F. Ma, L. Wang, X. Duan and S. Wang, *Environmental science & technology*,
947 2018, **52**, 8649-8658.
- 948 37. Y. Qin, G. Li, Y. Gao, L. Zhang, Y. S. Ok and T. An, *Water research*, 2018, **137**, 130-143.
- 949 38. M. Ahmad, A. U. Rajapaksha, J. E. Lim, M. Zhang, N. Bolan, D. Mohan, M. Vithanage, S. S. Lee
950 and Y. S. Ok, *Chemosphere*, 2014, **99**, 19-33.
- 951 39. A. D. Igalavithana, S. Mandal, N. K. Niazi, M. Vithanage, S. J. Parikh, F. N. D. Mukome, M. Rizwan,
952 P. Oleszczuk, M. Al-Wabel, N. Bolan, D. C. W. Tsang, K.-H. Kim and Y. S. Ok, *Critical Reviews in*
953 *Environmental Science and Technology*, 2017, **47**, 2275-2330.
- 954 40. X. Xiong, I. K. M. Yu, L. Cao, D. C. W. Tsang, S. Zhang and Y. S. Ok, *Bioresource technology*, 2017,
955 **246**, 254-270.
- 956 41. W.-J. Liu, H. Jiang and H.-Q. Yu, *Chemical Reviews*, 2015, **115**, 12251-12285.
- 957 42. J. Li, J. Dai, G. Liu, H. Zhang, Z. Gao, J. Fu, Y. He and Y. Huang, *Biomass and Bioenergy*, 2016, **94**,
958 228-244.

- 959 43. S. Wang, M. Zhao, M. Zhou, Y. C. Li, J. Wang, B. Gao, S. Sato, K. Feng, W. Yin, A. D. Igalavithana,
960 P. Oleszczuk, X. Wang and Y. S. Ok, *Journal of hazardous materials*, 2019, **373**, 820-834.
- 961 44. K. Luo, Q. Yang, Y. Pang, D. Wang, X. Li, M. Lei and Q. Huang, *Chemical Engineering Journal*,
962 2019, **374**, 520-530.
- 963 45. J. S. Cha, S. H. Park, S.-C. Jung, C. Ryu, J.-K. Jeon, M.-C. Shin and Y.-K. Park, *Journal of Industrial*
964 *and Engineering Chemistry*, 2016, **40**, 1-15.
- 965 46. A. U. Rajapaksha, S. S. Chen, D. C. W. Tsang, M. Zhang, M. Vithanage, S. Mandal, B. Gao, N. S.
966 Bolan and Y. S. Ok, *Chemosphere*, 2016, **148**, 276-291.
- 967 47. S. You, Y. S. Ok, S. S. Chen, D. C. W. Tsang, E. E. Kwon, J. Lee and C.-H. Wang, *Bioresource*
968 *technology*, 2017, **246**, 242-253.
- 969 48. J. Yan, L. Han, W. Gao, S. Xue and M. Chen, *Bioresource technology*, 2015, **175**, 269-274.
- 970 49. J. Lee, K.-H. Kim and E. E. Kwon, *Renewable & Sustainable Energy Reviews*, 2017, **77**, 70-79.
- 971 50. E. F. Zama, Y.-G. Zhu, B. J. Reid and G.-X. Sun, *Journal of Cleaner Production*, 2017, **148**, 127-
972 136.
- 973 51. G. Fang, C. Zhu, D. D. Dionysiou, J. Gao and D. Zhou, *Bioresource technology*, 2015, **176**, 210-217.
- 974 52. X. Ruan, Y. Sun, W. Du, Y. Tang, Q. Liu, Z. Zhang, W. Doherty, R. L. Frost, G. Qian and D. C. W.
975 Tsang, *Bioresource technology*, 2019, **281**, 457-468.
- 976 53. F. Beckers, Y. M. Awad, J. Beiyuan, J. Abridata, S. Mothes, D. C. W. Tsang, Y. S. Ok and J. Rinklebe,
977 *Environment International*, 2019, **127**, 276-290.
- 978 54. D. Zhong, Y. Jiang, Z. Zhao, L. Wang, J. Chen, S. Ren, Z. Liu, Y. Zhang, D. C. W. Tsang and J. C.
979 Crittenden, *Environmental science & technology*, 2019, **53**, 9034-9044.
- 980 55. Z. Wan, Y. Sun, D. C. W. Tsang, I. K. M. Yu, J. Fan, J. H. Clark, Y. Zhou, X. Cao, B. Gao and Y. S.
981 Ok, *Green Chemistry*, 2019, **21**, 4800-4814.

- 982 56. D. Zhong, Y. Zhang, L. Wang, J. Chen, Y. Jiang, D. C. W. Tsang, Z. Zhao, S. Ren, Z. Liu and J. C.
983 Crittenden, *Environmental Pollution*, 2018, **243**, 1302-1309.
- 984 57. X. Duan, H. Sun, Z. Ao, L. Zhou, G. Wang and S. Wang, *Carbon*, 2016, **107**, 371-378.
- 985 58. Y. Sun, C. Lei, E. Khan, S. S. Chen, D. C. W. Tsang, Y. S. Ok, D. Lin, Y. Feng and X.-d. Li,
986 *Chemosphere*, 2017, **176**, 315-323.
- 987 59. H. Dong, J. Deng, Y. Xie, C. Zhang, Z. Jiang, Y. Cheng, K. Hou and G. Zeng, *Journal of hazardous*
988 *materials*, 2017, **332**, 79-86.
- 989 60. H. Lyu, J. Tang, Y. Huang, L. Gai, E. Y. Zeng, K. Liber and Y. Gong, *Chemical Engineering Journal*,
990 2017, **322**, 516-524.
- 991 61. L. Lu, R. Shan, Y. Shi, S. Wang and H. Yuan, *Chemosphere*, 2019, **222**, 391-398.
- 992 62. F. Yang, S. Zhang, Y. Sun, K. Cheng, J. Li and D. C. W. Tsang, *Bioresource technology*, 2018, **265**,
993 490-497.
- 994 63. F. Yang, S. Zhang, H. Li, S. Li, K. Cheng, J.-S. Li and D. C. W. Tsang, *Chemical Engineering Journal*,
995 2018, **348**, 191-201.
- 996 64. M.-T. Yang, W.-C. Tong, J. Lee, E. Kwon and K.-Y. A. Lin, *Journal of colloid and interface science*,
997 2019, **545**, 16-24.
- 998 65. C. Lei, Y. Sun, D. C. W. Tsang and D. Lin, *Environmental Pollution*, 2017, **232**, 10.
- 999 66. H. S. Kambo and A. Dutta, *Renewable & Sustainable Energy Reviews*, 2015, **45**, 359-378.
- 1000 67. M. B. Ahmed, J. L. Zhou, H. H. Ngo, W. Guo and M. Chen, *Bioresource technology*, 2016, **214**,
1001 836-851.
- 1002 68. M. S. Khorram, Q. Zhang, D. Lin, Y. Zheng, H. Fang and Y. Yu, *Journal of Environmental Sciences*,
1003 2016, **44**, 269-279.
- 1004 69. M. Tripathi, J. N. Sahu and P. Ganesan, *Renewable & Sustainable Energy Reviews*, 2016, **55**, 467-
1005 481.

- 1006 70. M. I. Inyang, B. Gao, Y. Yao, Y. Xue, A. Zimmerman, A. Mosa, P. Pullammanappallil, Y. S. Ok and
1007 X. Cao, *Critical Reviews in Environmental Science and Technology*, 2016, **46**, 406-433.
- 1008 71. X. F. Tan, Y. G. Liu, Y. L. Gu, Y. Xu, G. M. Zeng, X. J. Hu, S. B. Liu, X. Wang, S. M. Liu and J. Li,
1009 *Bioresource technology*, 2016, **212**, 318-333.
- 1010 72. G. Agegnehu, A. K. Srivastava and M. I. Bird, *Applied Soil Ecology*, 2017, **119**, 156-170.
- 1011 73. C. Peiris, S. R. Gunatilake, T. E. Mlsna, D. Mohan and M. Vithanage, *Bioresource technology*, 2017,
1012 **246**, 150-159.
- 1013 74. N. A. Qambrani, M. M. Rahman, S. Won, S. Shim and C. Ra, *Renewable and Sustainable Energy*
1014 *Reviews*, 2017, **79**, 255-273.
- 1015 75. M. Vithanage, I. Herath, S. Joseph, J. Bundschuh, N. Bolan, S. O. Yong, M. B. Kirkham and J.
1016 Rinklebe, *Carbon*, 2017, **113**, 219-230.
- 1017 76. X. Ran, M. K. Awasthi, R. Li, J. Park, S. M. Pensky, W. Quan, J. J. Wang and Z. Zhang, *Bioresource*
1018 *technology*, 2017, **246**, 203.
- 1019 77. H. Wu, C. Lai, G. Zeng, J. Liang, J. Chen, J. Xu, J. Dai, X. Li, J. Liu and M. Chen, *Critical Reviews*
1020 *in Biotechnology*, 2016, **37**, 1-11.
- 1021 78. X. Zhu, B. Chen, L. Zhu and B. Xing, *Environmental Pollution*, 2017, **227**, 98-115.
- 1022 79. H. Bamdad, K. Hawboldt and S. Macquarrie, *Renewable & Sustainable Energy Reviews*, 2017, **81**,
1023 S1364032117309152.
- 1024 80. J. Wang and S. Wang, *Journal of Cleaner Production*, 2019, **227**, 1002-1022.
- 1025 81. K. N. Palansooriya, Y. S. Ok, Y. M. Awad, S. S. Lee, J.-K. Sung, A. Koutsospyros and D. H. Moon,
1026 *Journal of environmental management*, 2019, **234**, 52-64.
- 1027 82. A. El-Naggar, S. S. Lee, J. Rinklebe, M. Farooq, H. Song, A. K. Sarmah, A. R. Zimmerman, M.
1028 Ahmad, S. M. Shaheen and Y. S. Ok, *Geoderma*, 2019, **337**, 536-554.
- 1029 83. W.-D. Oh and T.-T. Lim, *Chemical Engineering Journal*, 2019, **358**, 110-133.

- 1030 84. T. Gagić, A. Perva-Uzunalić, Ž. Knez and M. Škerget, *Industrial & Engineering Chemistry Research*,
1031 2018, **57**, 6576-6584.
- 1032 85. B. Zhao, D. O'Connor, J. Zhang, T. Peng, Z. Shen, D. C. W. Tsang and D. Hou, *Journal of Cleaner*
1033 *Production*, 2018, **174**, 977-987.
- 1034 86. L. Yang, G. Liu, M. Zheng, R. Jin, Y. Zhao, X. Wu and Y. Xu, *Environmental science & technology*,
1035 2017, **51**, 12329-12336.
- 1036 87. X. Ruan, Y. Liu, G. Wang, R. L. Frost, G. Qian and D. C. W. Tsang, *Bioresource technology*, 2018,
1037 **270**, 223-229.
- 1038 88. A. D. Igalavithana, S. Wan Choi, P. D. Dissanayake, J. Shang, C.-H. Wang, X. Yang, S. Kim, D. C.
1039 W. Tsang, K. B. Lee and Y. S. Ok, *Journal of hazardous materials*, 2019, 121147.
- 1040 89. G. Fang, C. Liu, J. Gao, D. D. Dionysiou and D. Zhou, *Environmental science & technology*, 2015,
1041 **49**, 5645-5653.
- 1042 90. K. Marco, P. S. Nico, M. G. Johnson and K. Markus, *Environmental science & technology*, 2010,
1043 **44**, 1247-1253.
- 1044 91. M. Sevilla and A. B. Fuertes, *Carbon*, 2009, **47**, 2281-2289.
- 1045 92. D. A. Cantero, M. D. Bermejo and M. J. Cocero, *Bioresource technology*, 2013, **135**, 697-703.
- 1046 93. T. Kotake, H. Kawamoto and S. Saka, *Journal of Analytical & Applied Pyrolysis*, 2014, **105**, 309-
1047 316.
- 1048 94. N. Zhao, Z. Yin, F. Liu, M. Zhang, Y. Lv, Z. Hao, G. Pan and J. Zhang, *Bioresource technology*, 2018,
1049 **260**, 294-301.
- 1050 95. J. Qin, Q. Chen, M. Sun, S. Peng and G. Shen, *Chemical Engineering Journal*, 2017, **330**, 804-812.
- 1051 96. P. Gao, D. Yao, Y. Qian, S. Zhong, L. Zhang, G. Xue and H. Jia, *Environmental Chemistry Letters*,
1052 2018, **16**, 1463-1468.
- 1053 97. V. Eric, S. M. Lomnicki and D. Barry, *Environmental science & technology*, 2012, **46**, 9406.

- 1054 98. A. A. Peterson, F. Vogel, R. P. Lachance, M. Fröling, M. J. A. Jr and J. W. Tester, *Energy &*
1055 *Environmental Science*, 2008, **1**, 32-65.
- 1056 99. L. Klüpfel, A. Piepenbrock, A. Kappler and M. Sander, *Nature Geoscience*, 2014, **7**, 195.
- 1057 100. K. E. Miller, C.-T. Lai, E. S. Friedman, L. T. Angenent and D. A. Lipson, *Soil Biology and*
1058 *Biochemistry*, 2015, **83**, 176-183.
- 1059 101. E. D. Melton, E. D. Swanner, S. Behrens, C. Schmidt and A. Kappler, *Nature Reviews Microbiology*,
1060 2014, **12**, 797.
- 1061 102. A. Kappler and S. B. Haderlein, *Environmental science & technology*, 2003, **37**, 2714-2719.
- 1062 103. L. Klüpfel, M. Keiluweit, M. Kleber and M. Sander, *Environmental science & technology*, 2014, **48**,
1063 5601-5611.
- 1064 104. J. Yang, B. Pan, H. Li, S. Liao, D. Zhang, M. Wu and B. Xing, *Environmental science & technology*,
1065 2015, **50**, 694-700.
- 1066 105. T. Sun, B. D. A. Levin, J. J. L. Guzman, A. Enders, D. A. Muller, L. T. Angenent and J. Lehmann,
1067 *Nature Communications*, 2017, **8**, 14873.
- 1068 106. X. Li, L. Liu, X. Wang, Y. S. Ok, J. A. W. Elliott, S. X. Chang and H.-J. Chung, *Scientific reports*,
1069 2017, **7**, 1685.
- 1070 107. J. M. Saquing, Y. U. Yuhan and C. C. Pei, 2016, **3**, 62-66.
- 1071 108. D. Xin, M. Xian and P. C. Chiu, *Chemosphere*, 2019, **215**, 827-834.
- 1072 109. Y. Wu, J. Guo, Y. Han, J. Zhu, L. Zhou and Y. Lan, *Chemosphere*, 2018, **200**, 373-379.
- 1073 110. J. He, Y. Xiao, J. Tang, H. Chen and H. Sun, *Science of The Total Environment*, 2019, **690**, 768-777.
- 1074 111. L. Kemmou, Z. Frontistis, J. Vakros, I. D. Manariotis and D. Mantzavinos, *Catalysis Today*, 2018,
1075 **313**, 128-133.
- 1076 112. K. Zhu, X. Wang, M. Geng, D. Chen, H. Lin and H. Zhang, *Chemical Engineering Journal*, 2019,
1077 **374**, 1253-1263.

1078 113. H. Sun, S. Liu, G. Zhou, H. M. Ang, M. O. Tadé and S. Wang, *ACS applied materials & interfaces*,
1079 2012, **4**, 5466-5471.

1080 114. Y. Wang, Z. Ao, H. Sun, X. Duan and S. Wang, *Applied Catalysis B Environmental*, 2016, **198**, 295-
1081 302.

1082 115. D. Wu, W. Song, L. Chen, X. Duan, Q. Xia, X. Fan, Y. Li, F. Zhang, W. Peng and S. Wang, *Journal*
1083 *of hazardous materials*, 2020, **381**, 121010.

1084 116. C. Sun, T. Chen, Q. Huang, M. Zhan, X. Li and J. Yan, *Chemical Engineering Journal*, 2020, **380**,
1085 122519.

1086 117. Z. Jian, L. Xi, B. Raoul, Z. Aihua, S. G. Robert and S. D. Sheng, *Science*, 2008, **322**, 73-77.

1087 118. Y. Ma, W. J. Liu, N. Zhang, Y. S. Li, H. Jiang and G. P. Sheng, *Bioresource technology*, 2014, **169**,
1088 403-408.

1089 119. Z. Wan, M. Li, Q. Zhang, Z. Fan and F. Verpoort, *Environmental Science and Pollution Research*,
1090 2018, **25**, 17830-17841.

1091 120. H. Chen and K. C. Carroll, *Environmental Pollution*, 2016, **215**, 96-102.

1092 121. X. Duan, H. Sun, Y. Wang, K. Jian and S. Wang, *Acs Catalysis*, 2015, **5**, 553-559.

1093 122. J. Yang, J. J. Pignatello, B. Pan and B. Xing, *Environmental science & technology*, 2017, **51**, 8972-
1094 8980.

1095 123. W. Gehling and B. Dellinger, *Environmental science & technology*, 2013, **47**, 8172-8178.

1096 124. X. Dong, L. Q. Ma, J. Gress, W. Harris and Y. Li, *Journal of hazardous materials*, 2014, **267**, 62-70.

1097 125. A. L. N. Cruz, Dela, R. L. Cook, S. M. Lomnicki and D. Barry, *Environmental science & technology*,
1098 2012, **46**, 5971-5978.

1099 126. B. Dellinger, S. Lomnicki, L. Khachatryan, Z. Maskos, R. W. Hall, J. Adunkpe, C. McFerrin and
1100 H. Truong, *Proceedings of the Combustion Institute*, 2007, **31**, 521-528.

1101 127. F. Rodríguez-Reinoso, *Carbon*, 1998, **36**, 159-175.

- 1102 128. G. Fang, J. Gao, C. Liu, D. D. Dionysiou, Y. Wang and D. Zhou, *Environmental science &*
1103 *technology*, 2014, **48**, 1902-1910.
- 1104 129. J. Qin, Y. Cheng, M. Sun, L. Yan and G. Shen, *Science of The Total Environment*, 2016, **569-570**, 1-
1105 8.
- 1106 130. G. Fang, C. Liu, Y. Wang, D. D. Dionysiou and D. Zhou, *Applied Catalysis B: Environmental*, 2017,
1107 **214**, 34-45.
- 1108 131. J. Liu, S. Jiang, D. Chen, L. Liu, J. Wu and Y. Shu, *Chemical Engineering Journal*, 2019, 122637.
- 1109 132. C. B. Wang and W. X. Zhang, *Environmental science & technology*, 1997, **31**, 9602-9607.
- 1110 133. Y. Zhou, B. Gao, A. R. Zimmerman, H. Chen, M. Zhang and X. Cao, *Bioresource technology*, 2014,
1111 **152**, 538-542.
- 1112 134. D. Jiang, J. Xue, L. Wu, W. Zhou, Y. Zhang and X. Li, *Applied Catalysis B: Environmental*, 2017,
1113 **211**, 199-204.
- 1114 135. Q. Zhong, Q. Lin, R. Huang, H. Fu, X. Zhang, H. Luo and R. Xiao, *Chemical Engineering Journal*,
1115 2020, **380**, 122608.
- 1116 136. T. Zhang, Y. Chen, Y. Wang, J. Le Roux, Y. Yang and J. P. Croue, *Environmental science &*
1117 *technology*, 2014, **48**, 5868-5875.
- 1118 137. X. Duan, S. Indrawirawan, J. Kang, W. Tian, H. Zhang, X. Duan, X. Zhou, H. Sun and S. Wang,
1119 *Catalysis Today*, 2019, Doi: <https://doi.org/10.1016/j.cattod.2019.02.051>.
- 1120 138. J. Choi, H. Oh, S.-W. Han, S. Ahn, J. Noh and J. B. Park, *Current Applied Physics*, 2017, **17**, 137-
1121 145.
- 1122 139. A. Khataee, D. Kalderis, P. Gholami, A. Fazli, M. Moschogiannaki, V. Binas, M. Lykaki and M.
1123 Konsolakis, *Applied Surface Science*, 2019, 143846.
- 1124 140. J. R. Kim and E. Kan, *Journal of environmental management*, 2016, **180**, 94-101.

- 1125 141. P. Lisowski, J. C. Colmenares, O. Mašek, W. Lisowski, D. Lisovytskyi, A. Kamińska and D. Łomot,
1126 *ACS Sustainable Chemistry & Engineering*, 2017, **5**, 6274-6287.
- 1127 142. Y.-Y. Wang, H.-Y. Ji, H.-H. Lyu, Y.-X. Liu, L.-L. He, L.-C. You, C.-H. Zhou and S.-M. Yang, *Journal*
1128 *of Cleaner Production*, 2019, **231**, 556-564.
- 1129 143. L. Lin, Z. Song, Z. H. Khan, X. Liu and W. Qiu, *Science of The Total Environment*, 2019, **686**, 1185-
1130 1193.
- 1131 144. J. Guo, C. Yan, Z. Luo, H. Fang, S. Hu and Y. Cao, *Journal of Environmental Sciences*, 2019, **85**,
1132 168-176.
- 1133 145. L. Lin, W. Qiu, D. Wang, Q. Huang, Z. Song and H. W. Chau, *Ecotoxicology and Environmental*
1134 *Safety*, 2017, **144**, 514-521.
- 1135 146. V.-T. Nguyen, T.-B. Nguyen, C.-W. Chen, C.-M. Hung, C. P. Huang and C.-D. Dong, *Bioresource*
1136 *technology*, 2019, **292**, 121954.
- 1137 147. M.-T. Yang, Y. Du, W.-C. Tong, A. C. K. Yip and K.-Y. A. Lin, *Chemosphere*, 2019, **226**, 924-933.
- 1138 148. X. Chen, X. Duan, W.-D. Oh, P.-H. Zhang, C.-T. Guan, Y.-A. Zhu and T.-T. Lim, *Applied Catalysis*
1139 *B: Environmental*, 2019, **253**, 419-432.
- 1140 149. J. Ortiz-Medina, Z. Wang, R. Cruz-Silva, A. Morelos-Gomez, F. Wang, X. Yao, M. Terrones and M.
1141 Endo, *Advanced materials*, 2019, **31**, 1805717.
- 1142 150. J. Liang, X. Xu, W. Qamar Zaman, X. Hu, L. Zhao, H. Qiu and X. Cao, *Chemical Engineering*
1143 *Journal*, 2019, **375**, 121908.
- 1144 151. D. Ouyang, Y. Chen, J. Yan, L. Qian, L. Han and M. Chen, *Chemical Engineering Journal*, 2019,
1145 **370**, 614-624.
- 1146 152. M. Terrones, N. Grobert, J. Olivares, J. P. Zhang, H. Terrones, K. Kordatos, W. K. Hsu, J. P. Hare, P.
1147 D. Townsend, K. Prassides, A. K. Cheetham, H. W. Kroto and D. R. M. Walton, *Nature*, 1997, **388**, 52-
1148 55.

- 1149 153. T. Asefa and X. Huang, *Chemistry – A European Journal*, 2017, **23**, 10703-10713.
- 1150 154. X. Duan, S. Indrawirawan, H. Sun and S. Wang, *Catalysis Today*, 2015, **249**, 184-191.
- 1151 155. X. Duan, Z. Ao, H. Sun, S. Indrawirawan, Y. Wang, J. Kang, F. Liang, J. Zhu and S. Wang, *ACS*
1152 *applied materials & interfaces*, 2015, **7**, 4169.
- 1153 156. M. V. Nguyen and B. K. Lee, *Parocess Safety & Environmental Protection*, 2016, **104**, 490-498.
- 1154 157. X. Xu, Y. Zheng, B. Gao and X. Cao, *Chemical Engineering Journal*, 2019, **368**, 564-572.
- 1155 158. H. Sun, C. K. Kwan, A. Suvorova, H. M. Ang, M. O. Tadé and S. Wang, *Applied Catalysis B*
1156 *Environmental*, 2014, **154-155**, 134-141.
- 1157 159. M. Inagaki, M. Toyoda, Y. Soneda and T. Morishita, *Carbon*, 2018, **132**.
- 1158 160. X. Rong, M. Xie, L. Kong, V. Natarajan, L. Ma and J. Zhan, *Chemical Engineering Journal*, 2019,
1159 **372**, 294-303.
- 1160 161. W. Ma, N. Wang, Y. Du, P. Xu, B. Sun, L. Zhang and K.-Y. A. Lin, *ACS Sustainable Chemistry &*
1161 *Engineering*, 2019, **7**, 2718-2727.
- 1162 162. J. M. Chabu, L. Wang, F. Y. Tang, Z. Ke, J. Sheng, M. D. Walle, D. Liu and Y. N. Liu,
1163 *Chemelectrochem*, 2017, **7**, 19619-19625.
- 1164 163. W. Tian, H. Zhang, X. Duan, H. Sun, M. O. Tade, H. M. Ang and S. Wang, *ACS applied materials*
1165 *& interfaces*, 2016, **8**, 7184-7193.
- 1166 164. F. Lian, G. Cui, Z. Liu, L. Duo, G. Zhang and B. Xing, *Journal of environmental management*, 2016,
1167 **176**, 61-68.
- 1168 165. M. M. Mian, G. Liu, B. Yousaf, B. Fu, H. Ullah, M. U. Ali, Q. Abbas, M. A. Mujtaba Munir and L.
1169 Ruijia, *Chemosphere*, 2018, **208**, 712-721.
- 1170 166. F. Suo, X. You, Y. Ma and Y. Li, *Chemosphere*, 2019, **235**, 918-925.
- 1171 167. L. Tang, Y. Liu, J. Wang, G. Zeng, Y. Deng, H. Dong, H. Feng, J. Wang and B. Peng, *Applied*
1172 *Catalysis B: Environmental*, 2018, **231**, 1-10.

- 1173 168. S.-Y. Oh, J.-G. Son and P. C. Chiu, *Environmental Toxicology and Chemistry*, 2013, **32**, 501-508.
- 1174 169. S.-Y. Oh, J.-G. Son, O.-T. Lim and P. C. Chiu, *Environmental Geochemistry and Health*, 2012, **34**,
- 1175 105-113.
- 1176 170. T. Xue, S. Jiang, Y. Qu, Q. Su, R. Cheng, S. Dubin, C.-Y. Chiu, R. Kaner, Y. Huang and X. Duan,
- 1177 *Angewandte Chemie International Edition*, 2012, **51**, 3822-3825.
- 1178 171. S. Chen, A.-E. Rotaru, P. M. Shrestha, N. S. Malvankar, F. Liu, W. Fan, K. P. Nevin and D. R. Lovley,
- 1179 *Scientific reports*, 2014, **4**, 5019.
- 1180 172. Y. Dang, D. E. Holmes, Z. Zhao, T. L. Woodard, Y. Zhang, D. Sun, L.-Y. Wang, K. P. Nevin and D.
- 1181 R. Lovley, *Bioresource technology*, 2016, **220**, 516-522.
- 1182 173. J. Yu, L. Tang, Y. Pang, G. Zeng, J. Wang, Y. Deng, Y. Liu, H. Feng, S. Chen and X. Ren, *Chemical*
- 1183 *Engineering Journal*, 2019, **364**, 146-159.
- 1184 174. Z. Xu, X. Xu, X. Tao, C. Yao, D. C. W. Tsang and X. Cao, *Journal of hazardous materials*, 2019,
- 1185 **378**, 120705.
- 1186 175. X. Xu, H. Huang, Y. Zhang, Z. Xu and X. Cao, *Environ Pollut*, 2019, **244**, 423-430.
- 1187